M.W. Merritt, D. Klingle-Wilson, and S.D. Campbell

Wind Shear Detection with Pencil-Beam Radars

Abrupt changes in the winds near the ground pose serious hazards to aircraft during approach or departure operations. Doppler weather radars can measure regions of winds and precipitation around airports, and automatically provide air traffic controllers and pilots with important warnings of hazardous weather events. Lincoln Laboratory, as one of several organizations under contract to the Federal Aviation Administration, has been instrumental in the design and development of radar systems and automated weather-hazard recognition techniques for this application. The Terminal Doppler Weather Radar (TDWR) system uses automatic computer algorithms to identify hazardous weather signatures. TDWR detects and warns aviation users about low-altitude wind shear hazards caused by microbursts and gust fronts. It also provides advance warning of the arrival of wind shifts at the airport complex. Extensive weather radar observations, obtained from a Lincoln-built transportable testbed radar system operated at several sites, have validated the TDWR system. As a result, the Federal Aviation Administration has issued a procurement contract for the installation of 47 TDWR radar systems around the country.

Low-altitude wind shear has been a major cause of U.S. air carrier fatalities in recent years. A 1983 National Research Council study identified low-altitude wind shear as the cause of 27 aircraft accidents and incidents, with a total of 488 fatalities, between the years of 1964 and 1982 [1]. Since then, the National Transportation Safety Board investigated at least three additional wind shear incidents, including the crash of Delta Flight 191 at Dallas–Fort Worth on 2 August 1985, which claimed another 137 lives.

The Federal Aviation Administration (FAA) initiated the Terminal Doppler Weather Radar (TDWR) program in 1983. The purpose of this program is to procure a ground-based Doppler weather radar system for the automatic detection of wind shear hazards to aircraft, and to provide real-time warnings to air traffic controllers for relay to pilots. Future enhancements to the system will allow direct communication of warnings to pilots via radio data link.

Two primary forms of low-altitude wind shear present hazards to aircraft: the microburst and the gust front. The microburst is a strong short-lived outflow produced by strong thunderstorms. In certain regions of the country (for example, the Denver, Colo., area), even benign-looking clouds can produce microbursts. Gust fronts, also produced by thunderstorms, are defined as the boundary between the outflow from the storm and the ambient winds. While microbursts are short in duration (10 to 20 min) and occur with little warning, gust fronts can last for hours as they travel away from the generating storm system.

The detection of wind shear hazards presents challenges in three basic areas:

(1) the reliable measurement of horizontal winds, especially in low-signal, high-clutter environments;
(2) the automatic identification and classification of the hazardous weather signatures in the windfield measurements; and
(3) the assessment of the hazard level posed to aircraft, along with the effective communication of the hazard level to air traffic controllers and pilots, in a manner easily understood by these non-meteorologist users.

The emphasis in the weather radar program at Lincoln Laboratory has been on the first two of these areas. The effort has included the construction of a TDWR testbed radar system to collect test data from several meteorological environments across the country. The algorithm development cycle has included both off-line testing and real-time operational demonstrations.

Phenomenology of Microbursts and Gust Fronts

Downdrafts within storms generate microbursts and gust fronts. Through a variety of processes, including evaporative cooling and precipitation loading, negatively buoyant air within a storm descends to the ground as a downdraft. Upon reaching the surface, the downdraft spreads out horizontally from a divergent center and produces a pool of cold air known as the outflow [2].

Microbursts are formed when the divergence beneath the downdraft reaches a specified intensity, namely a change in wind speed of greater than 10 m/s over a distance of less than 4 km. Figure 1 illustrates a potentially hazardous encounter of a microburst by an aircraft on final approach. Upon entering the microburst, an aircraft first experiences an increase in head wind. This increase causes the aircraft to fly above the glide slope. The pilot, who is often unaware of the microburst, may attempt to return to the glide slope by reducing air speed and angle of attack. As the airplane continues through the microburst, it encounters a strong

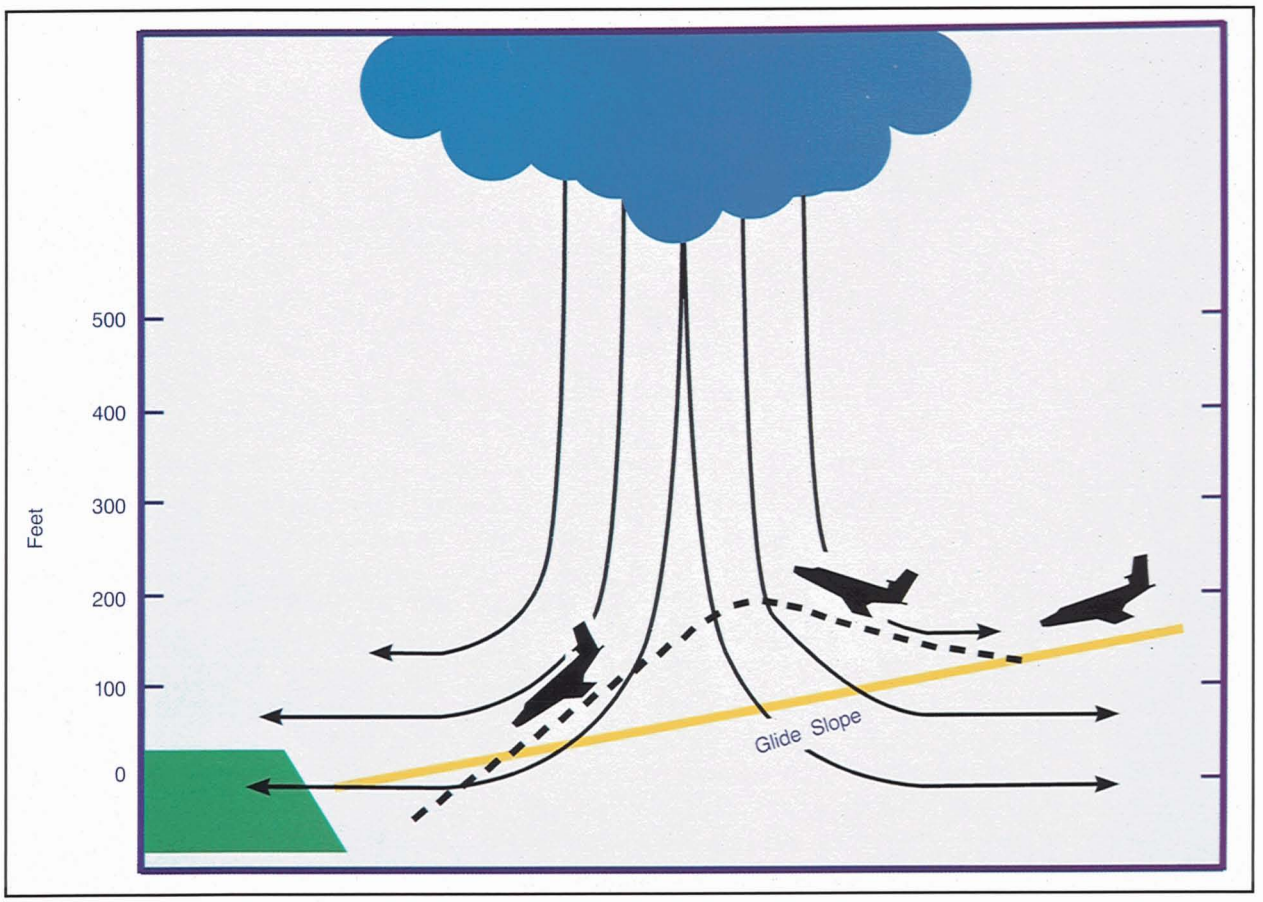

Fig. 1—Example of an aircraft encounter with a microburst. The spreading winds from a strong downdraft form the microburst outflow. A penetrating aircraft first experiences an increase in head wind, followed rapidly by a downdraft, and finally a tail wind. The loss in altitude across the event may result in ground impact.

downdraft and then a tail wind, which results in a loss of lift. The airplane falls beneath the glide slope and the pilot must now increase power and angle of attack to bring the plane back to the glide slope. The aircraft, which requires a finite amount of time to respond to the controls, crashes if it is too close to the ground to recover.

In most cases, the rain carried in the microburst provides a high-reflectivity signature. If the environment beneath the cloud base is dry, however, the precipitation evaporates before it reaches the ground, which results in a low-reflectivity signature. The evaporation also intensifies the microburst by further cooling the downdraft. The shape, size, and strength of the microburst shear region often evolve rapidly, particularly during the early growth of the outflow. When a strong downdraft first impacts the surface, it can change from a weak surface outflow to a strong microburst in a time period of 1 to 2 min. Most microbursts reach peak intensity and then decay in a time period of 10 to 20 min. More complicated events may pulse so that the microburst strength peaks and decays several times before the event dissipates completely.

The gust front is formed at the leading edge of the outflow, where the cooler air from the downdraft meets the warmer environmental air (Fig. 2). As the cool, dense outflow spreads out into the warm, less dense environmental air, horizontal convergence is produced at the outflow edge. During the passage of an outflow, an observer on the ground would experience a change from warm light winds to cool gusty winds (thus the name gust front). Gust fronts can last several hours, can propagate hundreds of kilometers from the parent storm, and commonly exist long after the parent storm has dissipated.

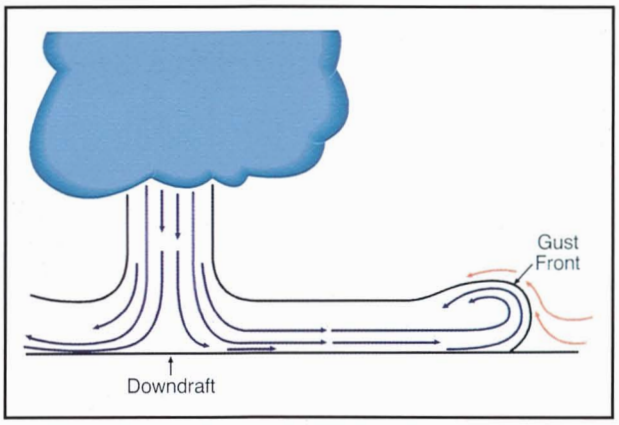

Fig. 2—An illustration of thunderstorm downdraft and outflow. The pool of cold air spread out beneath the storm is called the outflow. The gust front is the leading edge of the outflow where environmental and outflow winds converge.

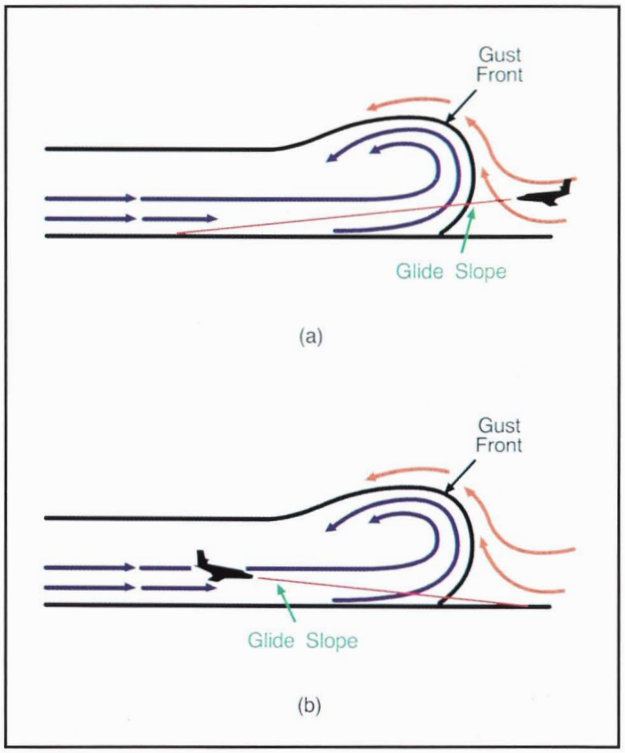

Fig. 3—Example of an encounter between a gust front and a landing aircraft. (a) As the aircraft flies into an outflow, it experiences an increase in head wind. (b) As the aircraft exits the outflow, it experiences a decrease in tail wind. Both situations result in a performance gain that causes the plane to rise above the glide slope. Strong turbulence may occur within the shear zone.

Gust fronts impact aviation in two ways: as a hazard to aircraft in flight and as a mechanism for creating delays in the terminal area. The gust front represents a transition zone of finite width between the cold (outflow) and warm (environmental) air masses. The strong surface winds, updrafts, and turbulence that exist within this zone may prove hazardous to an aircraft during takeoff and landing. Figure 3 illustrates the

conceptual model of an encounter between an aircraft and a gust front. In Fig. 3(a), the aircraft experiences an increasing head wind as it enters the outflow. In Fig. 3(b), the aircraft experiences a decreasing tail wind as it exits the outflow. The updrafts and turbulence asociated with the gust front often result in an uncomfortable ride. Both penetrations also result in a gain in aircraft performance that can cause an arriving plane to rise above the glide slope and overshoot the landing zone on the runway.

The passage of a gust front over an airport often produces a long-lasting change in the prevailing winds. The sudden wind shift can seriously impact the operation of the airport (for example, a change in wind direction would require runway changes). With advance notification of a wind shift, air traffic controllers can plan operations more effectively. The identification of the wind shift requires an estimation of the wind speed and direction behind the moving gust front boundary, typically in low-reflectivity regions.

Development of the TDWR System

In the late 1970s the FAA joined the National Weather Service and Air Weather Service in the development of a joint-use Next Generation Weather Radar system (NEXRAD) to provide contiguous weather radar coverage over the continental United States. The principal role for the NEXRAD system was to detect and monitor large severe storms, such as those that produce tornadoes. Late in the development of NEXRAD, scientific studies aimed at understanding the microburst wind shear phenomenon began to identify the characteristics of the hazard, as well as the radar system requirements for detection and warning of the hazards.

After the crash of Pan American Airlines flight 759 at New Orleans International airport (9 July 1982), the National Research Council conducted an in-depth examination of the aviation wind shear situation [1]. The study concluded that the FAA should develop a weather radar system that would be dedicated to identifying wind shear hazards in the airport terminal environment. While the technical characteristics of the NEXRAD radar were comparable to those deemed necessary for the terminal wind shear protection task, the joint-use mission of the NEXRAD radar prevented it from being sited and scanned in a manner appropriate to the terminal problem. The Terminal Doppler Weather Radar program was thus initiated, with the intent of using an enhanced NEXRAD-like radar tailored to the task of wind shear detection.

Lincoln Laboratory, already involved in the development of NEXRAD products for the FAA, began construction of a testbed radar system similar to NEXRAD to act as a data-collection and algorithm-evaluation facility for TDWR [3]. The ongoing scientific studies of wind shear phenomena, particularly the JAWS project [4] and the investigation of the crash of Pan Am flight 759 (both in 1982), led to a reorientation of the program at Lincoln Laboratory to focus on terminal wind shear hazards.

The testbed radar and algorithm development centered on microburst and gust front detection, and the first attempts at microburst data collection were made at MIT in 1983. To date, the testbed radar has been transported to several different sites where radar observations were performed on hundreds of microbursts. The radar was sited in Memphis, Tenn., during 1985, and then moved to Huntsville, Ala., for measurements during 1986. The radar observations made in Memphis and Huntsville provided the first operationally oriented study of microbursts in the humid southeast environment. Following the operations in Huntsville, the radar was relocated to Denver during 1987 and 1988. In 1988 the testbed was used to perform a complete Operational Test and Evaluation (OT&E) of the TDWR system. This OT&E (which Congress required to allow the procurement of the TDWR system to proceed) demonstrated that the TDWR, as specified, could provide a useful wind shear warning function for air traffic control.

The TDWR procurement was awarded to the

Raytheon Corporation in November of 1988. The first operational TDWR deliveries are scheduled to begin in volume in 1993. To obtain protection at critical airports before that date, the FAA contracted the NEXRAD supplier (Unisys) to adapt the initial 17 FAA-owned NEXRAD radars to perform as interim TDWR systems. This terminal variation of the NEXRAD radar will include only software modifications to run the TDWR algorithms. Initial terminal NEXRAD deliveries are scheduled to begin in 1990.

While the primary mission of the testbed radar system has been the development and evaluation of TDWR-related radar techniques and detection algorithms, the measurements from this radar have also been supplied to several national scientific studies on microburst phenomenology and storm-scale meteorology. During 1986, the radar operated as part of the COHMEX experiment [5], and the radar observations from Denver in 1987 were supplied to the CINDE program [6]. The ongoing data-collection program with the testbed radar has generated the most extensive collection of microburst and gust front radar data available, and has been of considerable benefit to the meteorological community.

While the Lincoln Laboratory testbed provided the radar observations for the development and testing of wind shear detection algorithms, the Research Applications Program at the National Center for Atmospheric Research (NCAR) actively addressed the user-interface issues and requirements for TDWR. NCAR formed a TDWR User Working Group composed of pilots, pilot group representatives, FAA air traffic controllers, administration representatives, and scientists and engineers working on the TDWR development. This group examined the various requirements of the TDWR users (for which the system represented a totally new capability), especially the types of information that pilots and controllers wanted and how this information would be presented. The User Working Group, which met three times over the course of the system development, was responsible for the specification of the current concepts of TDWR display and warning [7].

Requirements for the TDWR

The primary goal of the TDWR is to detect microburst wind shear hazards and to provide warnings of these hazards to air traffic control personnel for relay to pilots. The wind shear from a microburst presents a significant hazard to an aircraft only during low-altitude flight, such as approach and departure operations. The User Working Group concluded that microburst warnings were relevant to pilots while they were operating at altitudes below 1,000 ft above ground level (AGL). Given the nominal 3° glide slope used by most aircraft arrival operations, this altitude limit requires that warnings must be provided out to 6 km from the end of each runway.

The microburst detection must also be timely. The TDWR is required to provide pilots with a warning of hazardous wind shear at least 1 min prior to their encounter with the hazard. To meet this time requirement, the TDWR microburst-recognition algorithm is designed to provide an initial warning when the surface outflow is still weak (10 m/s or less). Since the TDWR updates the microburst warning once per minute, the algorithm provides a timely warning when the outflow reaches a hazardous level.

A major economic benefit of TDWR is the detection and prediction of wind-shift lines. The arrival of a wind-shift line at an airport has a significant impact on operations, since it can cause a change in the active runway configuration. For example, the direction of takeoffs and landings for a given runway might have to be reversed because of a wind shift. This reversal would reroute approaching aircraft and force departing aircraft to taxi to the other end of the runway.

To provide a useful product for runway configuration planning, the TDWR is required to generate a 20-min prediction of the arrival of a wind shift at the airport. To meet this prediction requirement, the TDWR must detect gust fronts to a range of about 60 km from the airport.

The TDWR must also detect gust front wind shears that impact the runways. Gust fronts in the terminal area, which are considered less hazardous than microbursts, create turbulence and substantial crosswinds that can affect aircraft performance.

Data Acquisition in the TDWR

The TDWR antenna scan strategy represents

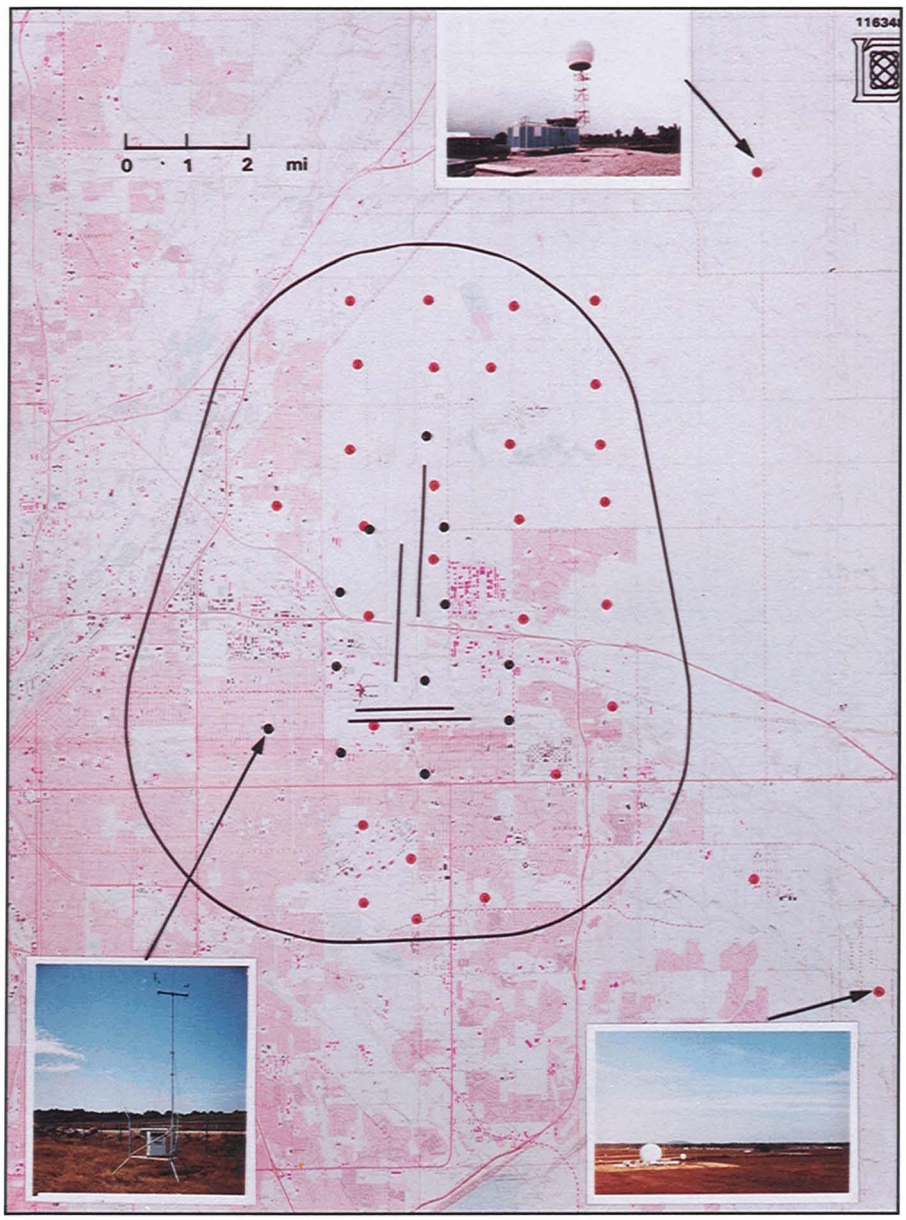

Fig. 4—Wind shear coverage region for the TDWR Operational Test and Evaluation at Stapleton Airport in Denver. The figure shows the airport runways and the oval-shaped radar coverage region that extends 6 km beyond the end of each runway. The inset photographs illustrate the Lincoln Laboratory testbed radar (15 km southeast of the airport), the University of North Dakota weather radar (northeast of the airport), and one of the mesonet surface wind-measurement stations. The red dots represent mesonet stations, while the blue dots represent locations for the FAA Low Level Wind Shear Alert System anemometer stations. The measurements recorded by these support instruments during the evaluation aided in the analysis of the meteorological events observed by the testbed radar.

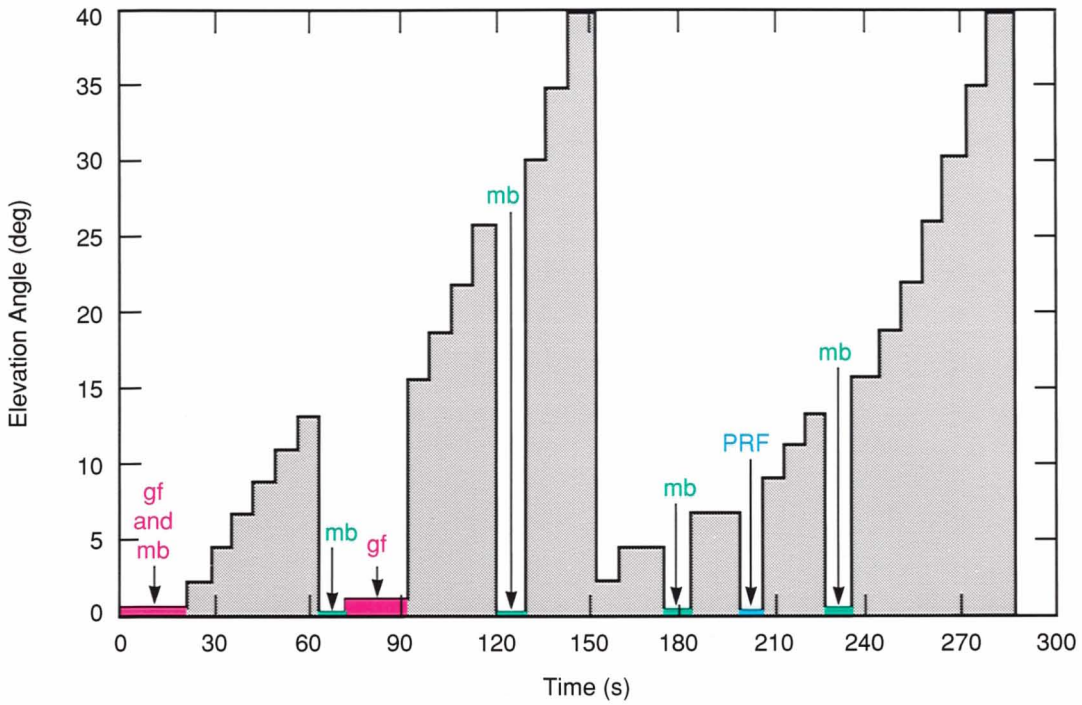

Fig. 5—Antenna elevation-angle sequence used for TDWR operational test and evaluation in 1988. The first scan in the sequence (shown in red) is a full-circle scan at an elevation of 0.5°. This scan is used jointly by the gust front and microburst algorithms. A second full-circle scan at an elevaion angle of 1° is used by the gust front algorithm alone. The microburst algorithm further requires surface scans at 1-min intervals. These scans (green) cover a 120° sector over the airport at an elevation angle of 0.4°. The PRF selection algorithm requires a long-range, low-PRF full-circle scan (blue). The remaining scans are used by the microburst precursor algorithm.

a complex trade-off of conflicting requirements by the various components of the detection and data-conditioning algorithms. The surface-divergence detection process, which is the primary component of the microburst-hazard detection system, requires updates of surface information at least once per minute. The feature-recognition algorithms for structures aloft require updates of the full storm volume, necessitating numerous scans at different elevation angles. Both of these detection algorithms require data only from the TDWR coverage region surrounding the airport and hence allow the radar to scan sectors on the order of 120° in width. Other algorithms, such as the gust front detection and automatic pulse repetition frequency (PRF) selection algorithm, require full-circle scans to identify gust fronts and storm cells in all directions [8].

Figure 4 illustrates the coverage region chosen for the TDWR OT&E in Denver during the summer of 1988. The center of the figure shows the airport runways, with the wind shear coverage region (which extends approximately 6 km off the end of each runway) shown as an oval outline. The figure also shows the location of the testbed radar and the supporting sensors. Figure 5 depicts the elevation angles chosen for this scan strategy. The elevation-angle sequence was chosen to meet the need for a 1-min surface update rate for the microburst algorithm, to meet the need for two full-circle surface scans every 5 min for the gust front algorithm, and to provide a worst-case vertical spacing from 1 km up to 6 km above ground level for observation of microburst features aloft.

This combination of scans provides frequent observations of the surface windfield, including one surface scan each minute, full-circle surface scans for gust front detection every 5 min,

and a top-to-bottom volume coverage every 2.5 min. The coverage of the volume above the airport area is important for the detection of microburst features aloft, particularly for the detection of storm reflectivity cores. The features aloft generally develop at altitudes of 5 to 6 km AGL and take several minutes to descend to the surface [9, 10]. The volume update rate achieved by the TDWR scan strategy allows observation of these descending core features at least twice during their descent, to provide early warning of incipient microbursts. The TDWR system continually repeats the scan strategy described above, and supplies the resulting radar measurements to the wind shear detection algorithms.

Because several forms of data contamination may affect the radar measurements, specific data-correction and data-editing procedures are applied prior to algorithm operation. The major forms of data contamination are ground-clutter residue, moving clutter, range aliasing, and velocity aliasing. Although the TDWR radar system must provide at least 50-dB ground-clutter rejection [11], the residue from strong clutter targets such as mountains or nearby buildings can result in data contamination. The TDWR employs a static ground-clutter residue map to edit the contaminated data regions [12]. The maps are created on clear days so that significant echoes can be associated with clutter residue and compared with operational measurements. When the operationally measured reflectivity levels compare to the clear-day echo levels, the data values are censored as contaminated. This approach edits data values coincident with strong clutter targets not removed by the high-pass filtering performed in the signal processor, except when sufficient weather power overcomes the clutter contamination. Moving clutter targets such as birds, airplanes, or automobiles are not rejected by the ground-clutter filtering, but are removed by a point-target rejection filter. The point-target rejection filter attempts to identify and delete spatially isolated discontinuities in the data. Careful filter design avoids editing the relatively small-scale microbursts that the system attempts to detect.

The effects of range aliasing and velocity aliasing are intrinsic to the pulsed Doppler weather radar sensor, since no single PRF can provide unambiguous measurements in both range and velocity (see the box titled "Range Aliasing and Velocity Aliasing with Pulsed Doppler Weather Radar"). The TDWR uses dynamic PRF selection logic to choose a PRF value that minimizes the amount of distant weather echoes to be range aliased into the significant observation regions for both microburst and gust front detection. Periodic low-PRF scans identify the long-range weather echoes, and the PRF for the operational scans is adjusted to handle the evolving out-of-trip weather pattern [13].

A complex combination of techniques addresses the velocity-aliasing problem. The TDWR testbed (which operates at S-band) utilizes software techniques to detect and correct velocity errors caused by aliasing [14]. These techniques rely on the spatial continuity of the velocity field, and attribute extremely large gate-to-gate velocity changes to aliasing. The production TDWR system will operate at C-band and hence be subject to more velocity aliasing. The TDWR contractor has designed a dual-PRF waveform to assist in the velocity de-aliasing process on those scans used for the wind-shift estimation algorithm (which is particularly sensitive to velocity errors).

Microburst Detection

The TDWR microburst detection process provides reliable and timely warnings by employing radar observations both at the surface and aloft. The surface velocity measurements first identify regions of divergence. If divergence regions are found, strength and temporal-continuity thresholds determine if the regions are significant enough to warrant the generation of microburst alarms. The detection of storm features aloft relaxes the strength and continuity requirements for alarm generation, and increases the likelihood that surface divergence regions will be considered as microbursts.

Figure 6 illustrates the three stages of processing modules in the detection algorithm: fea-

Range Aliasing and Velocity Aliasing with Pulsed Doppler Weather Radar

Pulsed Doppler weather radars use the pulse-to-pulse phase change of the received signal to estimate the radial velocity of the scatterers in the target sample volume. The phase-sampling approach results in a maximum unambiguous velocity beyond which the measured velocity is ambiguous (i.e. the phase change over a pulse period is greater than one-half wavelength). This maximum velocity, or Nyquist velocity, is given by

$$V = \frac{\lambda P}{4}$$

where λ is the radar wavelength and P is the radar pulse repetition frequency (PRF). The pulsed nature of the radar operation also introduces a maximum unambiguous range,

$$R = \frac{c}{2P}$$

(where c is the speed of light) beyond which the reflections from targets are incorrectly located in range. The radar wavelength, typically a fixed frequency for weather radars, couples these two aliasing effects as follows:

$$RV = \frac{c\lambda}{8}$$

The PRF (a variable operating parameter) adjusts the balance between the two effects. Figure A illustrates the set of range/velocity aliasing limits available to weather radars operating at various wavelengths (the Lincoln Laboratory testbed radar operates at S-band; the production TDWR will operate at C-band).

To reduce the possibility of range-aliased echoes from distant storms, the unambiguous range of a weather radar must be at least 450 km, where the radar horizon will extend above the tallest storm cells. To reduce the possibility of velocity aliasing, a velocity measurement range of at least ±35 m/s must be available for severe storm applications. Figure A illustrates this area of complete aliasing avoidance, where no range or velocity aliasing is likely to be experienced. The area is well outside of the achievable limits with either S- or C-band radars. As a result, practical weather radars must contend with both range- and velocity-aliasing effects.

Several techniques are available to reduce the data contamination effects from range and velocity aliasing in the weather radar context. The distributed nature of the weather targets (compared to more common discrete-target radar systems) is both a complication and an advantage for unfolding velocity measurements. Several software algorithms were developed that make use of the spatial continuity of weather measurements for velocity unfolding. Radar-waveform processing techniques can also deal with the aliasing problem, but careful system design is required to maintain a high level of ground-clutter rejection.

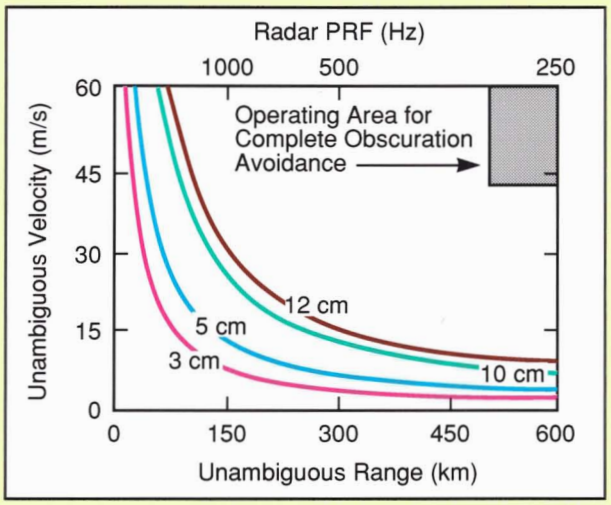

Fig. A—Trade-off between unambiguous range and velocity intervals. Each curve indicates the feasible operating points for the corresponding radar wavelength. The TDWR radar operates at C-band (5 cm); the Lincoln Laboratory testbed radar operates at S-Band (10 cm). Neither system is capable of operating free of both range and velocity aliasing.

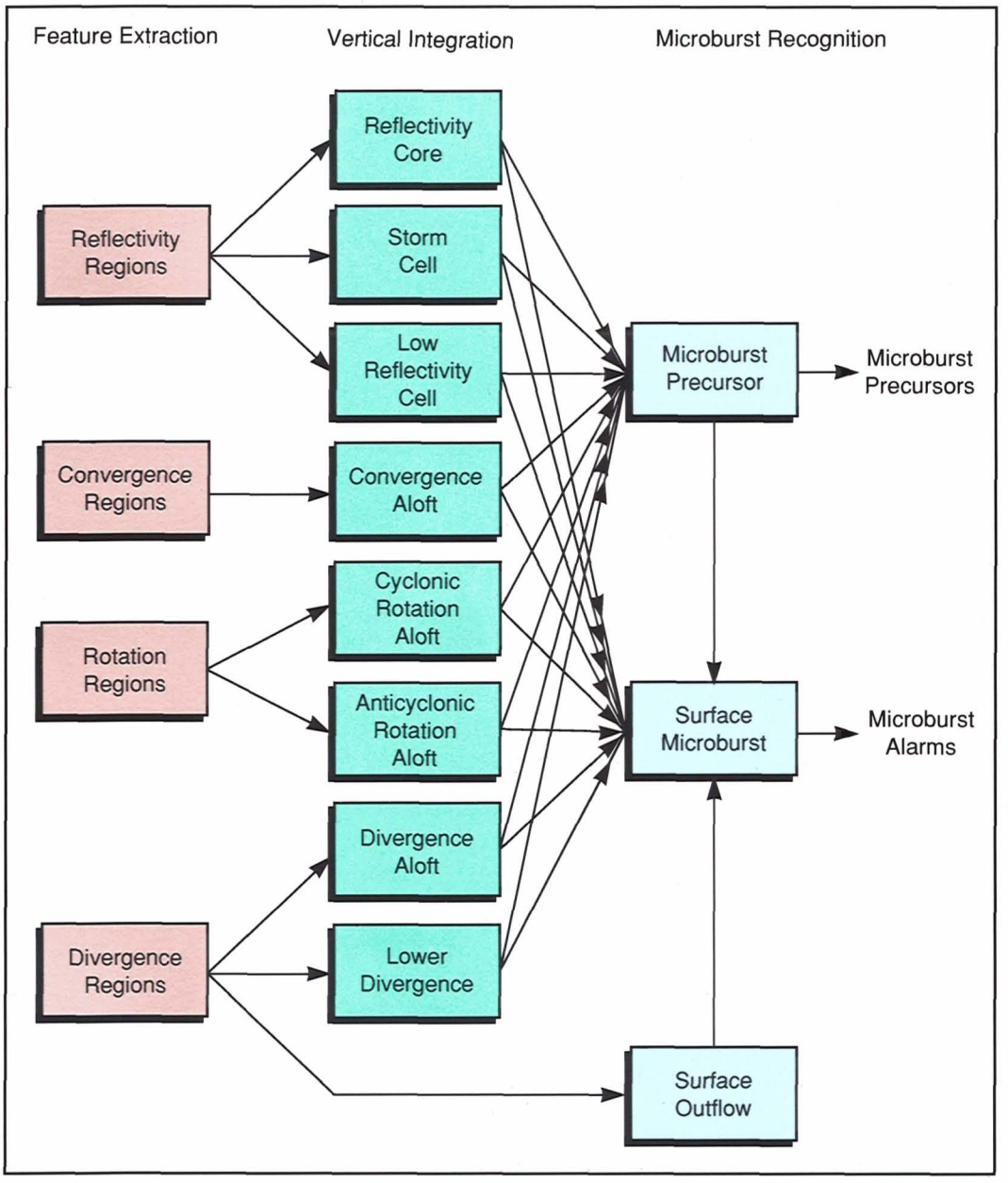

Fig. 6—The three microburst algorithm processing modules: feature extraction, vertical integration, and microburst recognition. The feature-extraction modules identify two-dimensional regions of convergence, divergence, rotation, and reflectivity. The vertical-integration modules assemble these regions into three-dimensional features aloft, such as a reflectivity core or convergence aloft. The microburst-recognition modules use these features aloft to identify microburst precursors and to aid the recognition of microburst surface outflows.

ture extraction, vertical integration, and microburst recognition. The feature-extraction modules identify two-dimensional regions of shear (divergence, rotation, and convergence) from base velocity data. Thresholding the base reflectivity field at several intensity levels (for example, 15, 30, and 45 dBz) also identifies regions of precipitation. These feature-extraction algorithm modules process the radar measurements made on each radar elevation scan.

The vertical-integration modules combine the regions identified from scans aloft into three-

dimensional reflectivity and velocity structures. Velocity structures include convergence aloft, rotation aloft, divergence aloft (storm top divergence), and lower divergence (above the surface but below 1 km AGL). Reflectivity structures include reflectivity cores, storm cells, and low-reflectivity cells.

The microburst-recognition modules consist of the surface-outflow, microburst-precursor, and surface-microburst algorithms. The surface-outflow algorithm attempts to identify microburst outflows by examining the temporal and spatial correlation of surface divergence features. The microburst-precursor algorithm attempts to recognize precursor signatures that indicate an imminent microburst, such as a descending reflectivity core coupled with a convergence aloft. The surface-microburst algorithm merges surface outflows with information about reflectivity structures, velocity structures, and precursor signatures to recognize microbursts.

The use of microburst precursors to augment surface outflows allows the detection algorithm to detect many microbursts earlier in time than would be possible with the outflow information alone. When significant precursor structures are identified, the algorithm declares a microburst alarm even when a very weak outflow is observed. This conditioning of the alarm thresholds often detects microbursts in their earliest stages, minutes before the outflow itself is sufficiently strong to trigger an alarm.

Microburst-Outflow Signatures and Their Detection

The divergence detection algorithm attempts to locate two-dimensional regions of divergent shear, based on radial-velocity measurements from the radar. The radial-velocity signature obtained from a divergent flow is simply a rapid increase with range of the radial velocity (where positive velocities indicate flow away from the radar). Figure 7 shows an example of such a signature. The color images in Fig. 7 illustrate the reflectivity field and the velocity field measured by the radar. Three microbursts are present in this data, outlined in red in the velocity field. Figure 7 also shows the velocity profile along a radial through the center of the strongest microburst. The divergence algorithm detected the section highlighted in red.

The algorithm scans the radial component of each velocity measurement to locate the shear signature, forming *shear segments* whenever a run of generally increasing velocity values is located. These shear segments are then associated across adjacent radials of the radar scan to form two-dimensional feature regions (Fig. 8).

The following description presents a brief outline of the divergence detection process [15]. The shear segments are identified by sliding a window out in range, typically 0.5 km in extent, and starting a segment when the velocity values in the window are monotonically increasing. Once the start of a segment is found, the end is determined by moving the window out farther in range as the values in the window generally continue to increase. This trend terminates when at least three-quarters of the sample points in the window have a velocity value less than the value at the first point in the window.

Each segment is then subjected to an iterative series of validation tests. On each iteration of the validation process, the segment end points are adjusted to insure that they are reasonable local extrema and have adequate slope or shear. After adjustment, the segment is tested to insure that it has adequate length and a consistent positive trend. Finally, each end point is tested to insure that its velocity value is close to the local median velocity value. If the shear segment passes all of these tests, it is accepted; otherwise the test is repeated until the segment is accepted or rejected.

The segments that survive these validation tests are then associated across radar azimuths to form two-dimensional regions of shear. Any two segments that exhibit adequate overlap in range (at least 0.5 km) and are within 2° in azimuth are joined together in the same region. The association process continues until all segments have been separated into regions. The aggregates are now thresholded based on their total area, number of segments, and maximum segment strength. Regions with area less than 1 square km, with fewer than 3 segments, or

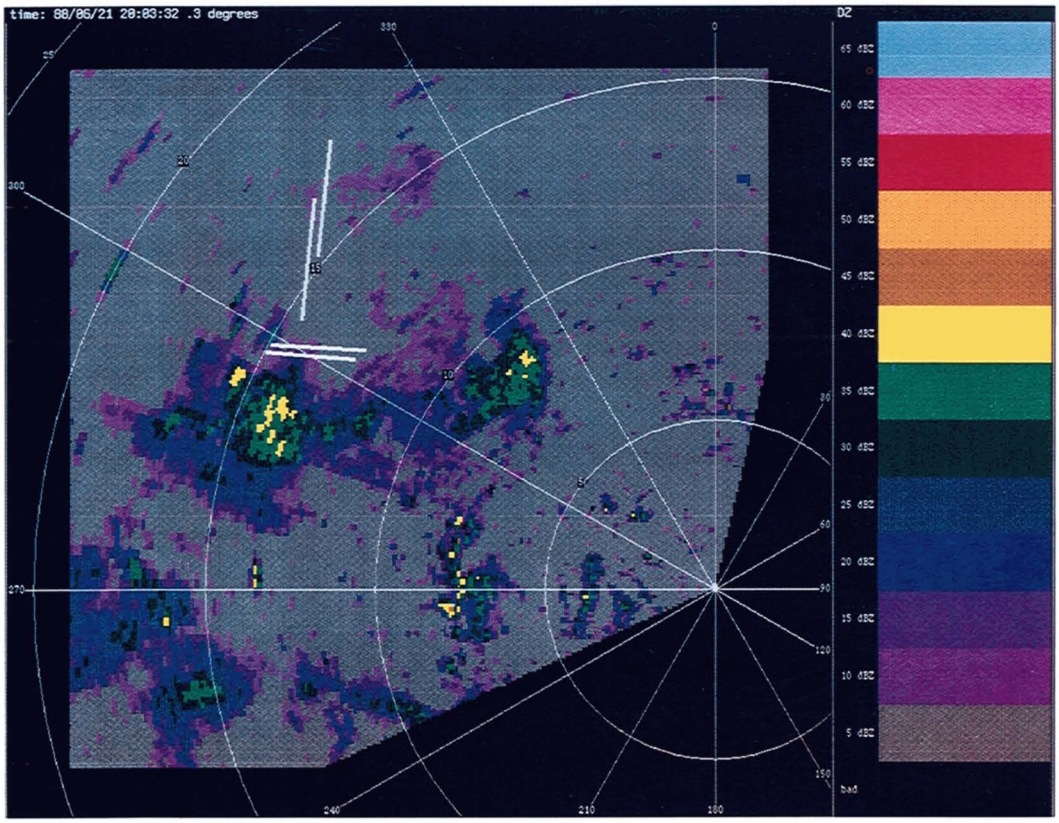

Fig. 7—Radar signature of microburst outflow. (above) The radar reflectivity field for a strong microburst recorded on 21 June 1988 in Denver. (facing page) The radial-velocity field for the same microburst. The reflectivity image is in units of dBz, and velocity values are in m/s (negative values indicate velocities toward the radar). The region outlined in red is microburst outflow. Note the region of aliased velocities in the velocity image at range 8 km and azimuth 310°. The Nyquist velocity for this data is ±18 m/s; the strong velocities in the microburst outflow have exceeded this limit. (below) The velocity profile through the center of the microburst shows a characteristic divergence signature of outflow along a radar radial at azimuth 313.5° for the case shown in the figure above. The portion of the velocity profile detected by the divergence algorithm is highlighted in red.

with a maximum velocity differential (across the strongest segment in the cluster) less than 5 m/s are discarded. The clustering process results in a set of significant regions of divergent shear, which are then passed to the three-dimensional vertical-association and time-continuity modules.

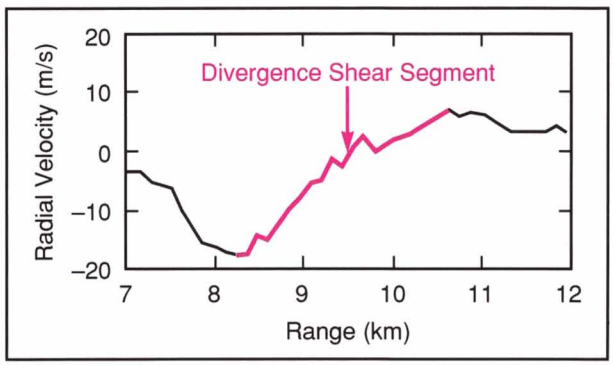

Microburst Features Aloft and Their Detection

In addition to surface outflow, microbursts are also associated with reflectivity and velocity features aloft. These features aloft can aid the recognition of surface outflows and can also serve as microburst precursors. A microburst

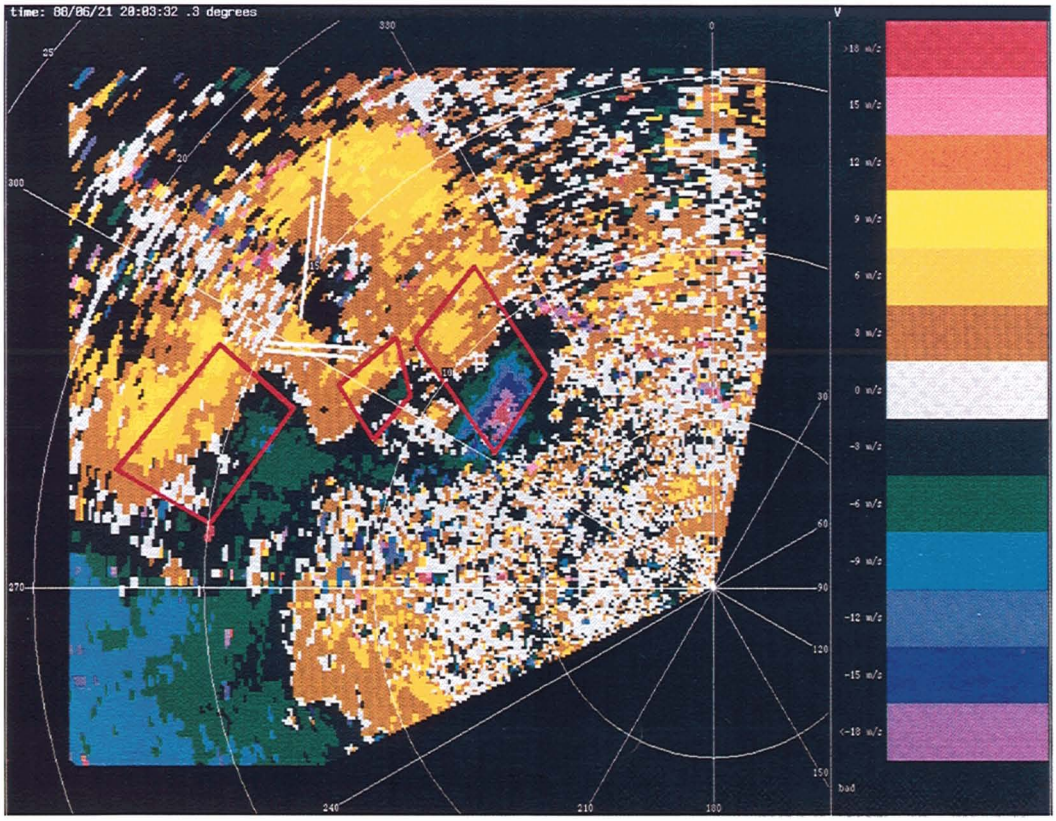

precursor is a set of features aloft that indicates the surface outflow will occur in 5 to 10 min.

Figure 9 shows a conceptual diagram for a microburst typically found in the southeastern United States. In the first stage of development, a reflectivity core appears aloft (at about 5 km AGL) in the parent storm of the microburst. At the same time, a convergence or inflow begins to develop at or above the level of the reflectivity core. In the second stage of development, the reflectivity core begins to sink to middle level (about 3 km). Convergence is evident now at this level and rotation often develops. Taken together, the descent of the reflectivity core and the development of the middle-level velocity signatures indicate that a strong downdraft has developed. The strong downdraft will produce the hazardous outflow at the surface. In the third stage of development, the reflectivity core reaches the surface, and divergent flow at the surface is now evident. Thus features aloft can allow the algorithm to declare the microburst outflow at an earlier stage than can be done with surface data only. Additional algorithm development may use these features aloft to generate forecasts of surface outflows, prior to actual divergence at the surface.

Figure 10 illustrates the detection procedure for a microburst on 7 June 1986 at Huntsville, Ala. The bottom graph shows the time course of the surface outflow as determined by the algorithm and by an expert observer. The graph shows that the event is declared in a timely fashion and is detected at all times when the outflow velocity exceeds the microburst-alert threshold of 15 m/s. The upper two graphs of Fig. 10 show the velocity and reflectivity features aloft detected by the algorithm. The upper and lower altitude limits for each structure are shown as a function of time. The initial microburst-precursor declaration is made at about 1642 GMT, based on the detected rotation aloft and reflectivity core signatures. The reflectivity core descends over the next 9 min, and reaches

the surface at 1651 GMT when the initial surface outflow of 8 m/s is observed (convergence aloft is also detected at this time).

On the basis of the precursor signature detected from the reflectivity core and the rotation aloft, the algorithm declared the microburst at 1651 GMT, rather than on the succeeding scan. For this case, the early declaration improved the timeliness of the microburst alarm by over 1 min, and the precursor signature was declared 9 min in advance of the surface outflow.

Gust Front Detection and Wind-Shift Estimation

Although gust fronts are often associated with thin lines of weak reflectivity and/or enhanced spectrum width, the most consistent and easily identifiable gust front signature is radial convergence in the Doppler velocity field. Figure 11 provides an example of a thunderstorm outflow and gust front as seen by a Doppler radar. Figure 11 (left) shows the gust front as a thin line of weak reflectivity in the reflectivity field. Figure 11 (middle) shows the outflow as the region of positive velocities in the Doppler-velocity field. Figure 11 (right) shows the linear signature of the gust front in the spectrum-width field. The gust front is the curve that separates the outflow from the ambient air. The red line in the figure represents the gust front as detected by the algorithm.

The gust front algorithm, originally developed at National Severe Storms Laboratory (NSSL) in 1984 [16] and continuously upgraded and improved since that time, detects gust fronts by using Doppler velocity alone [17]. The gust front algorithm consists of two separate algorithms: the gust front detection algorithm and the wind-shift estimation algorithm. For simplicity and

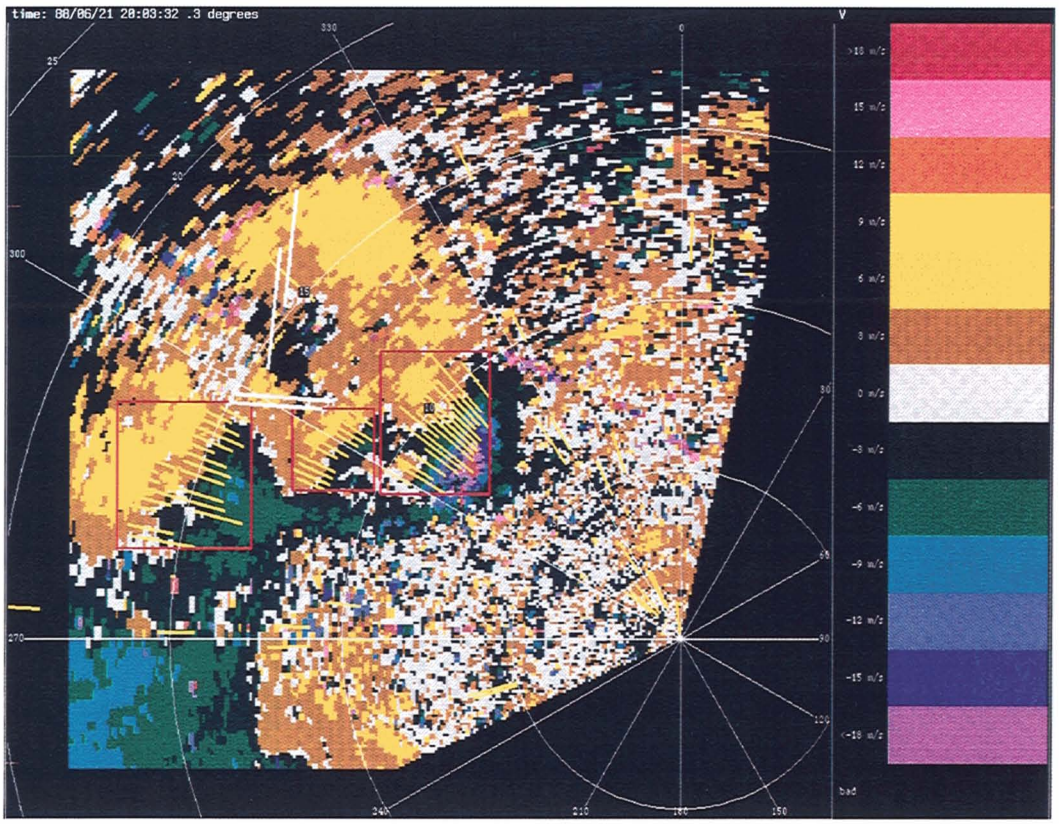

Fig. 8—Association of divergence shear segments into two-dimensional divergence regions. Primitive shear segments are shown in yellow, and resulting divergence regions in red.

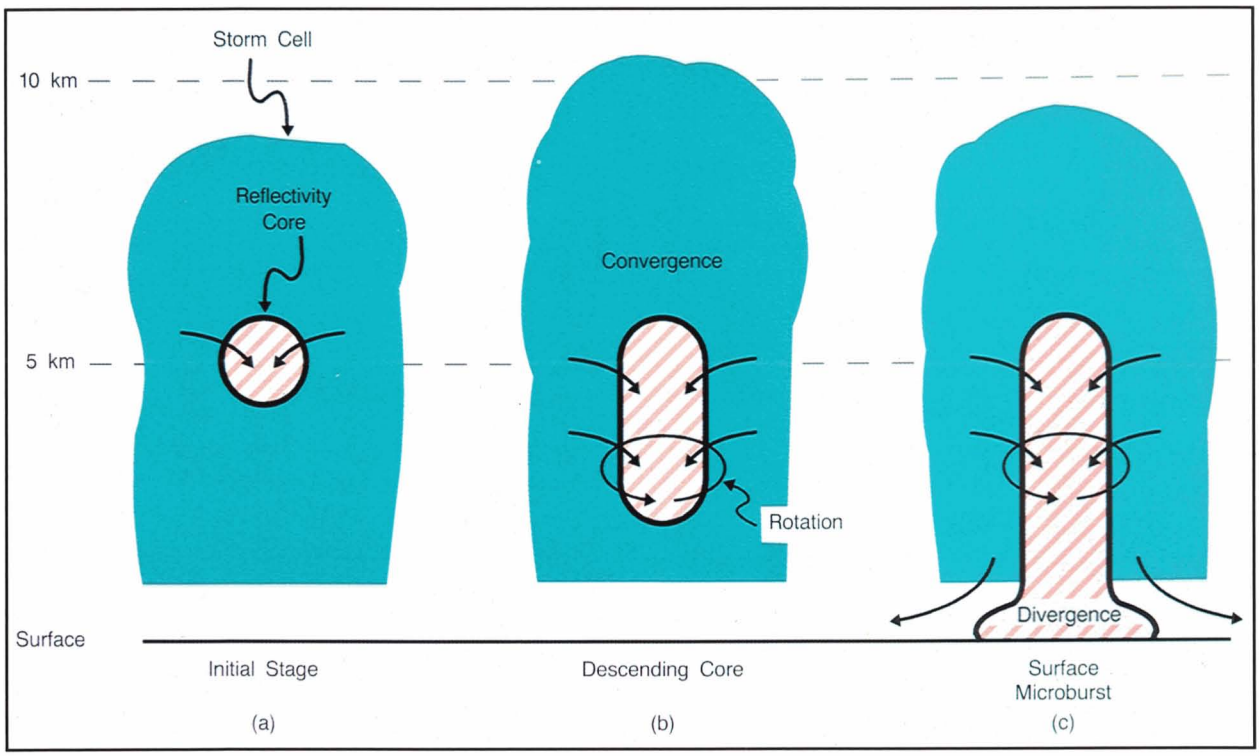

Fig. 9—Stages in the evolution of a microburst. (a) A reflectivity core initially forms aloft at 5 to 10 min prior to the onset of surface outflow. (b) As the downdraft develops, the core descends, and convergence and rotation develop. (c) Finally, the core reaches the surface and the surface outflow begins.

convenience, these algorithms are together called the gust front algorithm. This algorithm serves two functions: wind shear estimation for aircraft warning, and wind-shift estimation and forecasting for airport configuration planning. Wind shear warnings are issued when a gust front impacts the runways or within 6 km of the ends of the runways. The planning function alerts an ATC supervisor when a change in wind speed and/or direction caused by a gust front will occur at the airport within 20 min. The outputs of the algorithm are (1) a line identifying the location and shape of the gust front, (2) an estimate of the winds behind the gust front, (3) forecasts of the location of the gust front, and (4) an estimate of the wind shear an aircraft will experience as it encounters the gust front.

The gust front algorithm processes two full-circle scans (called *tilts*) during each volume update of the antenna scan strategy. The elevation angles of the tilts are typically 0.5° and 1.0°. The gust front algorithm uses pattern-recognition techniques to identify gust fronts in the radial-velocity field. For each tilt, the algorithm searches along radials for segments of decreasing radial velocity, which indicates radial convergence or shear (Fig. 12). If the value of the shear associated with each segment passes specified thresholds, the segments are stored for further processing.

Shear segments are grouped on the basis of proximity into features that are tested against thresholds and either discarded, kept, or combined with other features. After separately processing both tilts, the algorithm tests for vertical continuity between the tilts. If the algorithm establishes vertical continuity and the resulting feature passes a length threshold, a gust front detection is declared. Gust front location is determined by fitting a line through the locations of the peak shears along all shear segments that constitute the gust front. Peak shear is the maximum decrease in radial velocity that occurs over a distance of 1 km along

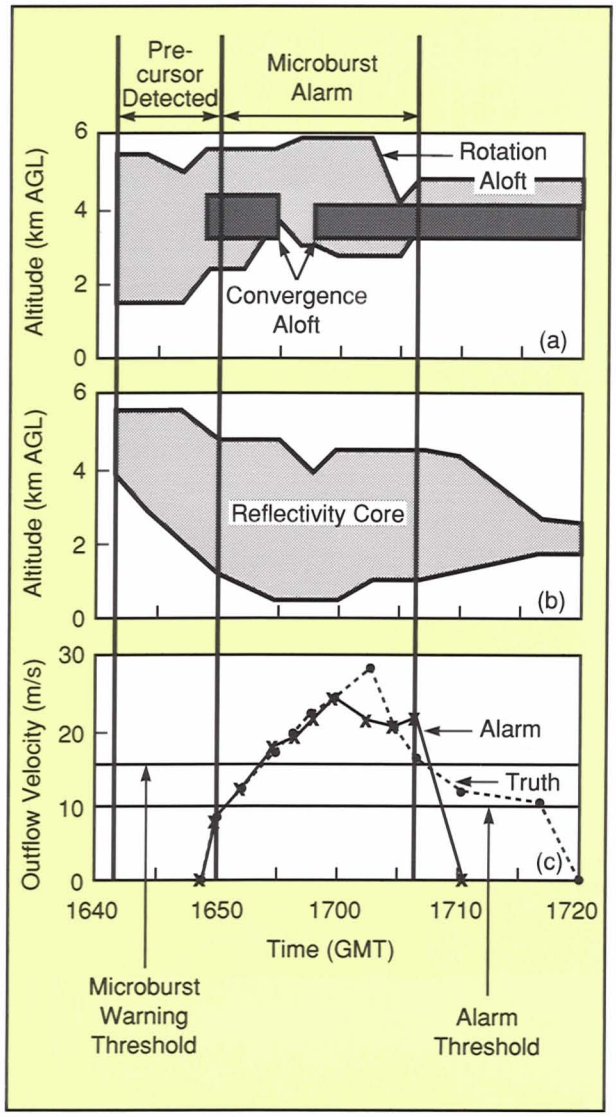

Fig. 10—Example of the use of microburst features aloft. The microburst algorithm detected the surface outflow and features aloft for an event observed by the Lincoln Laboratory testbed radar on 7 June 1986 at Huntsville, Ala. (a) Velocity features aloft detected by the algorithm; (b) reflectivity features aloft detected by the algorithm; (c) surface outflow as detected by the algorithm and determined by an expert observer. In this case, a microburst-precursor detection was made 9 min prior to the onset of surface outflow. The precursor is used to make an early declaration of the surface outflow, which increases the timeliness of the alarm.

a given shear segment.

The estimate of the wind shear that an aircraft might experience upon penetrating a gust front is derived from the peak shear. The mean and standard deviation of the peak shears of all shear segments in a gust front are computed. The wind shear estimate is simply the sum of these statistics.

To produce a forecast of the gust front location, the motion of the gust front with time must be established, which requires detections of the same gust front in two consecutive volume scans (Fig. 13). The centroid of each detection on each volume scan is computed. The algorithm calculates the distance between the centroids on consecutive volume scans and, if this distance passes a threshold, the detections are identified as the same gust front.

To generate a forecast, gust front propagation must be estimated. Gust fronts tend to propagate perpendicular to their orientations, so the component of the centroid-to-centroid vector perpendicular to the orientation is computed. The magnitude of the perpendicular component is divided by the time difference between consecutive detections to derive propagation speed. Propagation direction is parallel to the perpendicular-component vector. The forecast is simply the current detection moved along the propagation direction by a distance defined by the propagation speed multiplied by the desired forecast time (typically 10 and 20 min).

The gust front algorithm attempts to estimate the wind speed and direction ahead of and behind the gust front. The algorithm uses data from the 0.5° tilt and assumes a uniform horizontal wind within specified spatial sectors. Estimates of the wind components are obtained by regressing the smoothed Doppler velocities within each sector onto sine and cosine functions, and minimizing the sum of the squared errors between the measurements and the fitted values [18].

Alarm Generation

After the detection algorithms process the data, detections are sent to the display system for alarm generation (NCAR developed the requirements for this portion of the system, as well as the operational implementation used during the TDWR OT&E). The display system generates two types of user displays: a geographic situ-

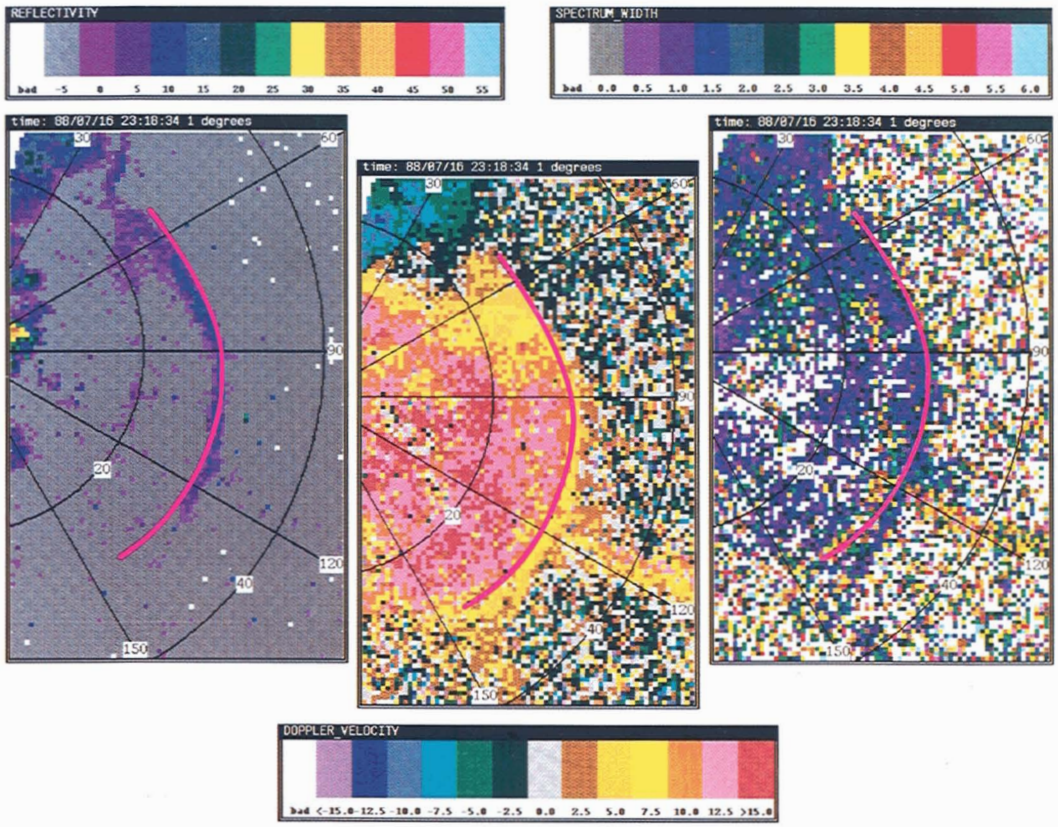

Fig. 11—An example of a thunderstorm gust front as seen by single Doppler radar. The gust front is identifiable as (left) a thin line of weak reflectivity, (middle) a linear region of radial convergence in the Doppler wind field, and (right) a linear feature in the spectrum-width field.

ation display (GSD) and an alphanumeric display. Airport tower supervisors and Terminal Radar Approach Control (TRACON) controllers use the GSD to understand the overall weather conditions impacting airport terminal operations. Local controllers use the alphanumeric display for alarm messages to be read directly to pilots. Figure 14 shows examples of both the GSD and alphanumeric displays [19].

To display microbursts, the display system first computes a smooth shape to represent the alarm region. The shape is constrained to a rectangle with semicircular ends (like a bandaid) that best fits the alarm region. Averaging is also performed with previous alarm regions to reduce the minute-by-minute jitter in the alarm size and location. The bandaid shapes are used to generate the GSD display of the microburst alarms.

To display gust front detections, the display system connects the series of points that describe the location of the gust front. The estimate of the wind speed behind the gust front is rounded to the nearest 5 knots and displayed as an alphanumeric character behind the front. Wind direction is shown by an arrow. The display software uses the most recent detection and the gust front propagation speed to compute the forecasted locations, and then displays the forecasted locations as dashed lines. The detected and predicted gust front locations are propagated each minute on the display, to update the gust front product along with the microburst displays.

To provide the alphanumeric warning messages, the display system intersects the shapes and lines of a microburst or gust front with the airport complex. The airport complex consists of

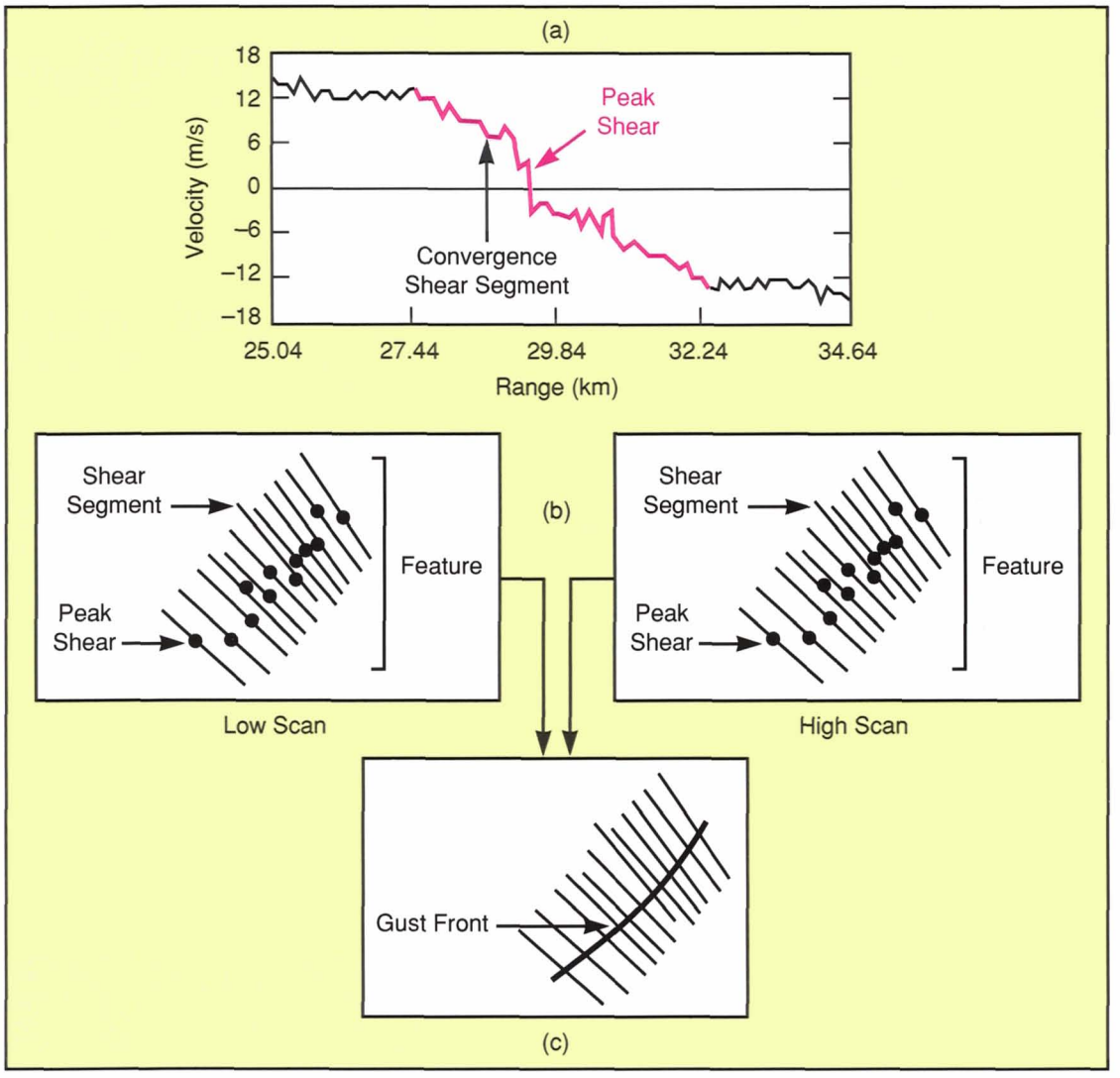

Fig. 12—Diagram illustrating gust front detection. (a) Radial-velocity data are searched for segments of decreasing Doppler velocity, which indicates radial convergence. The dots represent the locations of the peak shears along each segment. (b) Segments from the low (0.5) and high (1.0) tilts are grouped respectively into features, and (c) features are grouped on the basis of spatial proximity into gust fronts.

the area enclosed within a 1-km buffer zone on either side of the runway and 6 km past the end of the runway. If an intersection occurs, the system generates an alphanumeric alert for that runway, indicating the strength and location of the alarm with respect to the runway. Since a microburst is currently considered more hazardous to an aircraft than a gust front, a microburst alarm has priority over a gust front alarm on the same runway.

Evaluation of Wind Shear Detection Performance

Performance evaluation has been a major component of the wind shear algorithm development. Numerous performance evaluations were conducted to establish the absolute level of performance of the detection algorithms and to identify relative benefits of alternate algorithm approaches. A formal operational test and

evaluation of the TDWR system was conducted at Stapleton Airport in Denver during the summer of 1988. The system output products were then sent to on-duty air traffic controllers at Stapleton for evaluation.

During the operational evaluation, the testbed TDWR system was operated each day from noon to 7 PM. All base radar observations were routinely recorded and all TDWR system alarms and products were archived for subsequent analysis. Human observers monitored the weather situation and visually examined the radar measurements for wind shear events. For post-mission analysis, the observers kept detailed logs that noted the presence of wind shear events. Figures 15(a) and 15(b) provide a summary of the number of microbursts and gust fronts that were noted by these observers over the course of the evaluation period.

Fig. 14—Displays for TDWR. The color display on the left is the geographical situation display (GSD) used by tower and TRACON supervisors. It depicts location of wind shear and wind-shift events as well as storm regions. The alphanumeric display on the right is for local controllers. It provides runway-oriented text messages to be read directly to pilots.

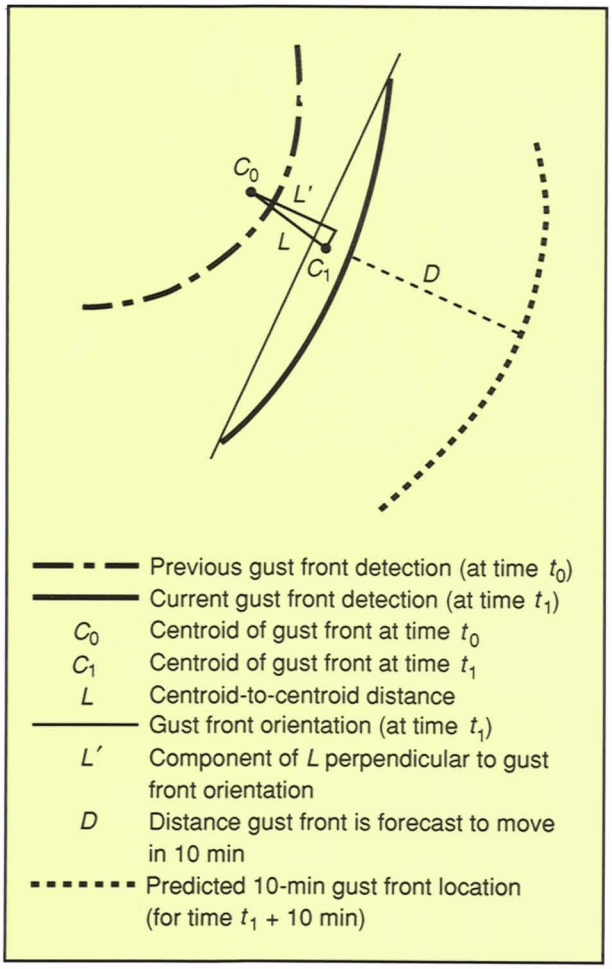

Fig. 13—Diagram illustrating gust front prediction. For each detection, the orientation and centroid location of the detection are computed. The location of the previous (t_0) detection, whose centroid is C_0, is shown by the dash-dot curve. The location of the current (t_1) detection, whose centroid is C_1, is shown by the solid curve. The orientation of the current detection is given by the thin solid line. L is the centroid-to-centroid distance and L′ is the component of L that is perpendicular to the orientation. D is the distance the gust front is expected to travel in 10 min; the dashed curve indicates the expected location of the gust front in 10 min.

Two methods determined the performance level of the wind shear algorithms during the evaluation. The first method, described as a *technical* evaluation, compared the wind shear alarms to human-generated ground-truth data that indicated the actual location of microburst or gust front events. This method of comparison is the primary metric for the ongoing development and reporting of algorithm performance. The second method, described as an *operational* evaluation, compared system alarms with reports from pilots who were operating at Stapleton during the evaluation period.

Technical Scoring Approach

The technical performance evaluation compares the wind shear alarms generated by the

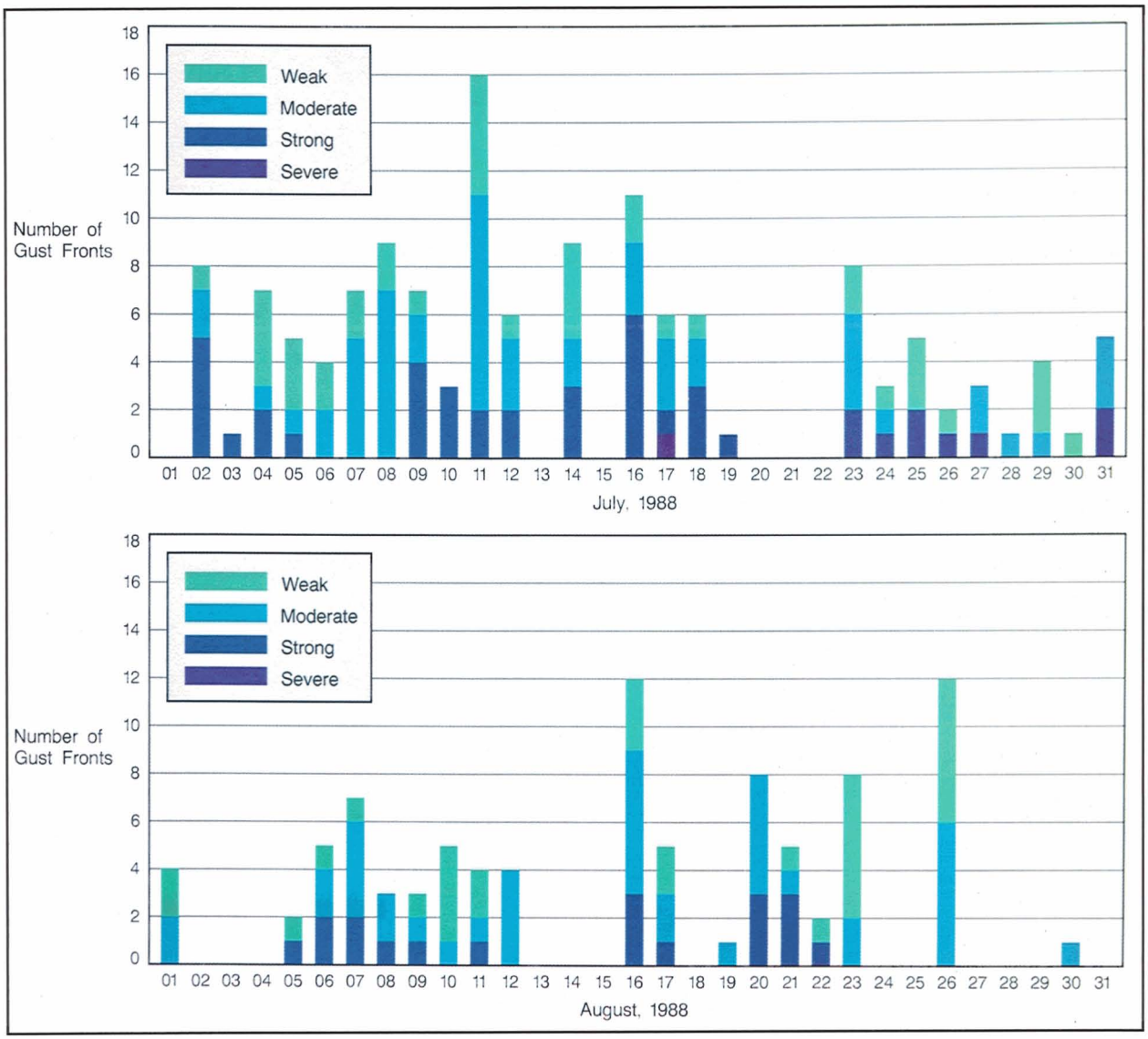

Fig. 15 (a)—A summary of gust front occurrences from the TDWR OT&E during July and August 1988.

microburst and gust front algorithms with reference (or ground truth) alarms generated by careful human analysis of the radar measurements. The ground-truth data base was created by using the base radar measurements from the testbed radar (the data input to the detection algorithms) along with data from other sensors such as surface wind stations and a second Doppler radar.

The algorithm performance is quantified by two basic statistics: the *probability of detection* (POD) and the *probablity of false alarm* (PFA), which are defined as follows:

$$\text{PFA} = \frac{\text{false alarms}}{\text{correct alarms + false alarms}}.$$

$$\text{POD} = \frac{\text{detected events}}{\text{total events}}$$

The definitions relate performance to three fundamental concepts: an *event*, a *detection*, and a *false alarm*. These basic terms can be defined in several ways to quantify different aspects of the performance of a system. To provide an operationally significant measure of the behavior of the wind shear detection system as it would appear to an end user (for example,

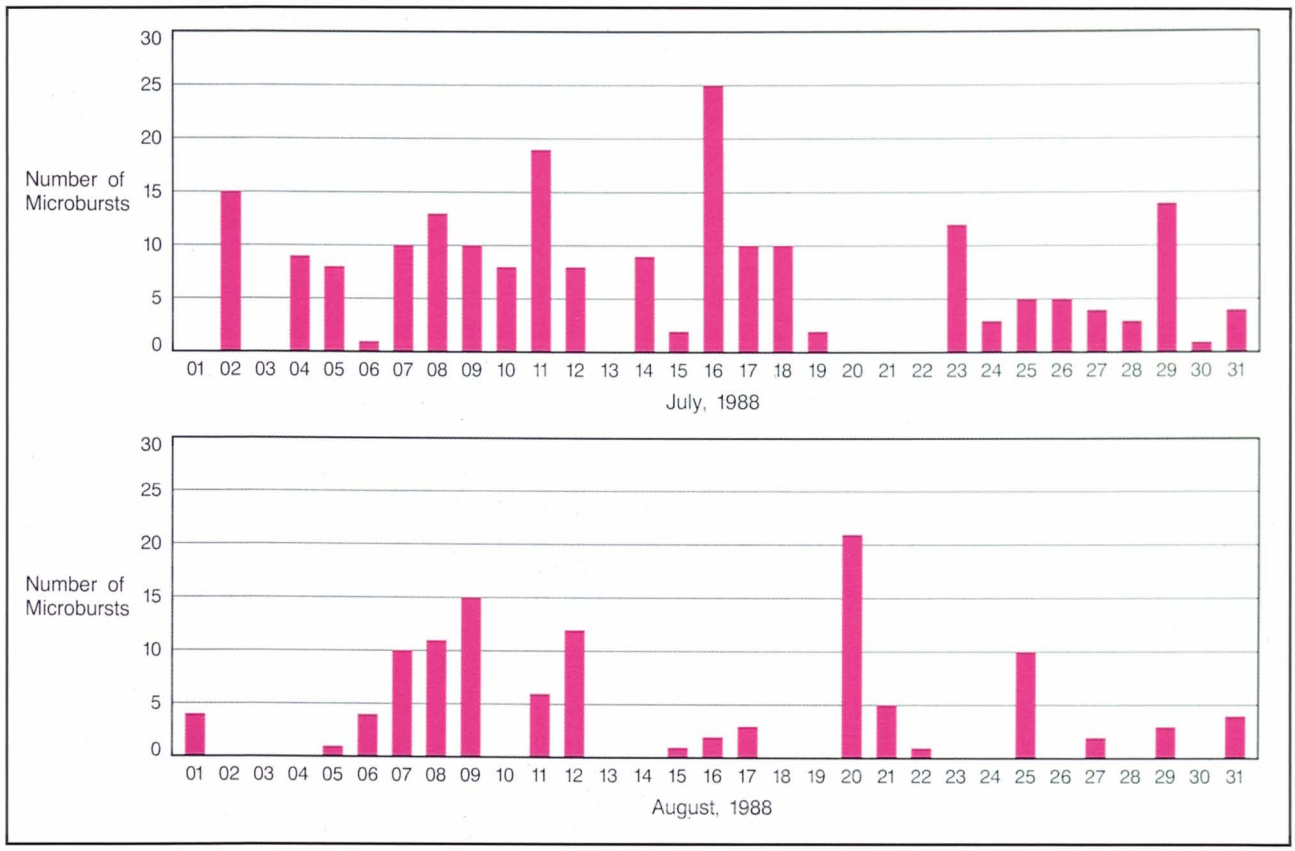

Fig. 15 (b)—A summary of microburst occurrences from the TDWR OT&E during July and August 1988.

an aircraft pilot), the following definitions have been used.

Event—A wind shear event is defined as a single observation (by the ground-truth analyst) of a microburst or gust front in the radar data on a low-elevation scan. Each microburst or gust front is typically observed on several sequential scans and hence represents several events. Only those microbursts that fall within a 10-km radius of the airport are considered in the scoring. Microburst events that are partially inside the 10-km limit are scored if 10% or more of the total event area, or at least 1 square km, whichever is smaller, falls within 10 km. All gust front events located within 60 km of the radar are scored.

Detection—A microburst or gust front event is considered a detection if its area is overlapped by a corresponding ground-truth event.

False Alarm—A gust front declaration is considered a false alarm if no ground-truth events overlap the area of the alarm. A microburst declaration is considered a false alarm if the ground-truth events overlap less than 10% of the area of the alarm. Otherwise, an alarm is considered correct.

The POD and PFA statistics describe the performance of target detection systems. The spatially distributed nature of the wind shear hazards, however, makes these simple detection statistics inadequate to describe completely the behavior of the detection algorithms. The existing scoring techniques do not explicitly quantify how timely the detections are (i.e., how soon the alarms start relative to the onset of the hazard over the airport region), how completely the hazard region is detected, or whether the hazard regions are detected one-for-one by the algorithms (i.e., splitting and merging of alarms). The assessment of algorithm performance in

these areas is difficult, and a matter of ongoing study.

The following sections describe in more detail the generation of ground truth and the technical scoring results for the microburst and gust front algorithms.

Microburst Algorithm Performance Assessment

The performance of the microburst detection algorithm during the TDWR OT&E was evaluated by using ground-truth information from single-Doppler radar analyses performed at Lincoln Laboratory. Table 1 lists the days for which ground truth was generated for the 1988 cases.

The single-Doppler ground truth was created by manually observing the radar-measured radial windfield and drawing polygonal outlines around the microburst-outflow regions in the data. This manual analysis task required detailed examination of each radar surface scan (once per minute) for the duration of each case day scored. A total of 475 scans were analyzed in this way. Figure 16 shows an example of a single-Doppler ground-truth case. The figure illustrates the truth outline for a strong microburst, along with the alarm generated by the detection algorithm for the same event.

To compute the POD and PFA statistics, the ground-truth microburst outlines are compared to the alarms generated by the microburst algorithm. Table 1 shows these statistics. The single-Doppler ground-truth cases achieved an overall POD of 90% with a PFA of 2%. Table 2 shows the POD as a function of microburst strength, and indicates that almost all of the algorithm misses are for weak microburst events (those with a wind-speed difference of less than 15 m/s). Very few misses occur for events with a wind-speed difference of 15 m/s or greater. Fortunately, the algorithm is more reliable for the stronger events that are more hazardous to aviation. The events missed by the algorithm occur primarily at the start or end of a microburst's lifecycle, when the microburst outflow is weakest.

Gust Front Algorithm Performance Assessment

As stated previously, the operational demonstration was conducted 7 hours per day for 60 days. With a volume update rate of 5 min, the

Table 1. Single-Doppler Ground Truth Cases Analyzed for 1988 Data

Date	*Number of Microbursts*	*Number of Events**	*POD(%)*	*PFA(%)*
10 June	17	158	85	4
21 June	17	213	93	1
25 June	12	169	95	3
7 July	10	102	87	0
17 July	6	58	88	4
Total	62	700	90	2

*Note: The number of events indicates the number of scan-by-scan observations of the microbursts by the radar. Each microburst is typically observed on about ten consecutive one-minute scans. The POD and PFA statistics are based on the ability of the algorithm to detect each individual event.

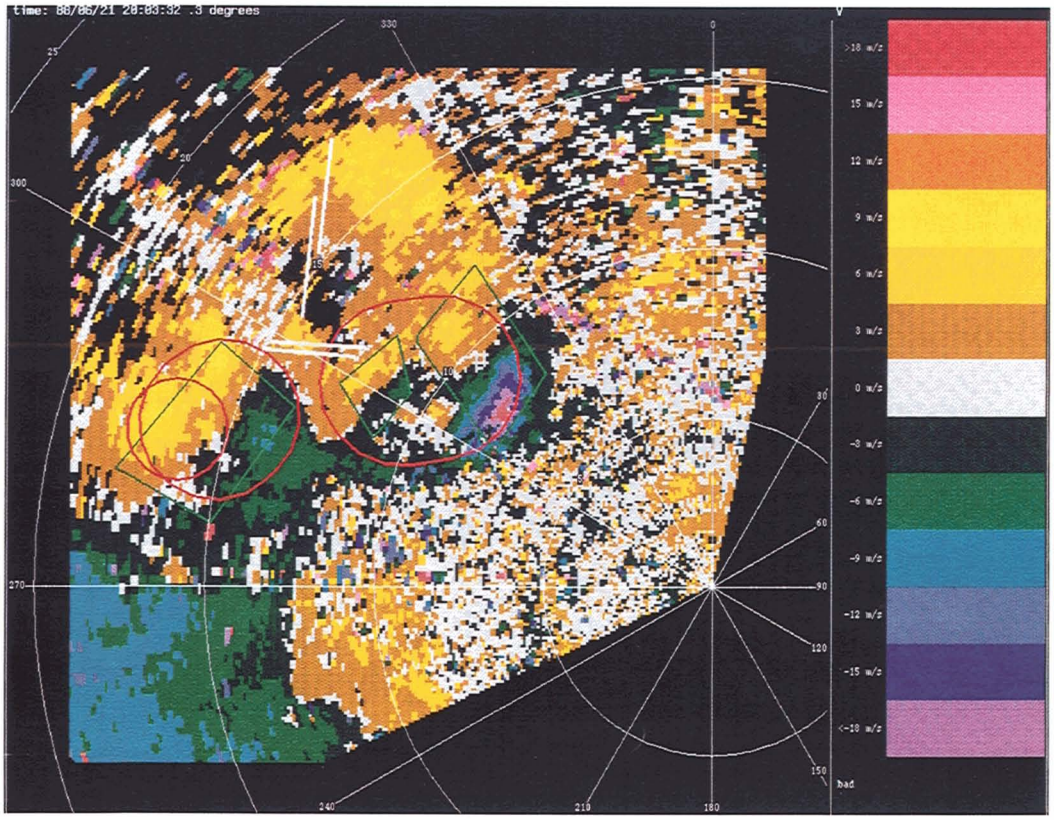

Fig. 16—Example of microburst ground truth from single-Doppler data. The green outline denotes a ground-truth region as determined by manual examination of the velocity field (shown in units of m/s). The red outline indicates the alarm generated by the microburst detection algorithm.

gust front algorithm processed over 5,000 low-angle tilts. Each tilt potentially contained one or more gust fronts. The goal of the gust front algorithm performance assessment was to truth and score, in near real time, every gust front event observed by the radar during the operational demonstration. To meet this ambitious goal in a timely manner, ground truth was generated during real-time operations and the scoring procedures were automated. Though the output of the algorithms was archived easily during operations, the real-time creation of a ground-truth data base and the automation of the scoring process required a significant software development effort.

Ground Truth

The gust front algorithm generated five products (detections, forecasts, wind-shift estimates, and location and intensity of wind shear alerts), each of which had to be scored. For the detections, forecasts, and locations of the wind shear alerts, the true locations of all gust fronts were needed. Ground truth for gust front location consisted of a series of points along the entire length of the gust front. The gust fronts were further categorized by strength. The strength (ΔV) of the gust front was the average peak change in Doppler velocity perpendicular to and along the convergent portion of the gust front. Gust fronts were defined as weak (5 m/s $\leq \Delta V <$ 10 m/s), moderate (10 m/s $\leq \Delta V <$ 15 m/s), strong (15 m/s $\leq \Delta V <$ 25 m/s), and severe ($\Delta V \geq$ 25 m/s). Radar meteorologists from NSSL and Lincoln Laboratory generated real-time ground truth, based on evidence of gust front signatures (radial convergence, azimuthal shear, and reflectivity thin line in single-Doppler radar data).

Table 2. Microburst Detection Performance as a Function of Outflow Strength

Date	Weak events (<15 m/s)	POD(%) (weak)	Strong events (>15 m/s)	POD(%) (strong)
10 June	78	71	80	99
21 June	115	87	98	100
25 June	42	81	127	99
7 July	51	77	51	98
17 July	11	36	47	100

Ground truth for the wind-shift algorithm was derived from surface wind measurements made by 38 portable weather stations located around the airport [20]. This network of weather stations was called a *mesonet*. Winds ahead of the gust front were available to ATC via the Low Level Wind Shear Alert System; thus only the estimate of wind speed and direction behind the gust front was displayed and scored. Since mesonet data constituted ground truth, only those wind shifts associated with gust fronts that passed through the mesonet were scored. To determine which mesonet stations were behind a gust front, the location of the gust front from single-Doppler radar data was superimposed on the plotted mesonet data. Those stations which had experienced a change in wind speed and/or direction were used for analysis. The wind direction computed by the algorithm was compared to the average wind direction from the mesonet. The algorithm-computed wind speed was compared to the average of the peak mesonet wind speeds that occurred during a 1-min interval. Pilot reports, recorded by observers located in the tower, determined ground truth for the wind shear alert intensities.

Scoring Definitions, Rules, and Results

Representing the gust front ground-truth outline by a straight line introduces errors into the representation of the gust front location. The gust front is a transition zone that is often not well represented by a line. The difficulty inherent in identifying the precise location of the peak shear, and the use of straight line segments rather than curves to connect the points, also introduces errors. To compensate, truth is represented by a box 5 km wide and centered on the straight line segments. Figure 17 illustrates such a truth box.

The POD, defined as the number of true detections divided by the number of gust fronts, measures algorithm performance. A true detection is declared when any part of a gust front is detected. Table 3 shows the POD as a function

Table 3. Probability of Detection of Gust Fronts

Moderate	Strong	Severe	All
73%	91%	100%	78%

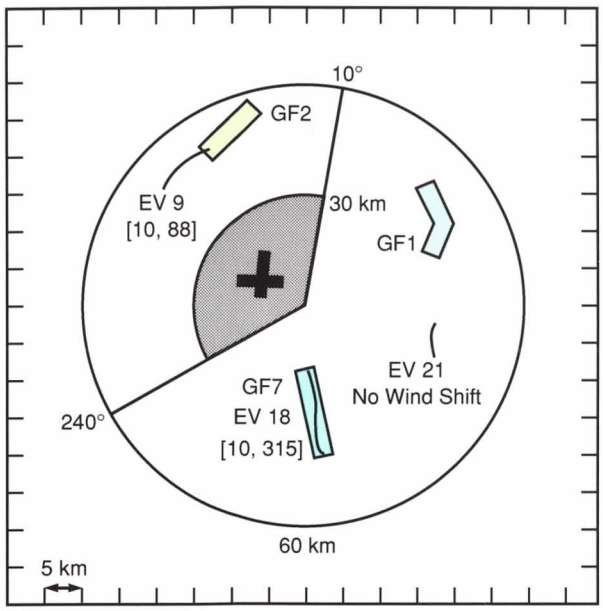

Fig. 17—Diagram illustrating truth, detections, and false alarms. The 5-km-wide boxes represent ground truth, and the solid lines represent detections. GF1 is an example of a missed gust front (truth with no associated detection). EV21 is an example of a false alarm (detection not associated with truth). The shaded area is the airport sector. The values in square brackets are estimates of wind speed and direction behind the front.

of gust front strength.

The PFA is defined as the number of false detections divided by the total number of detections (true plus false). The PFA for the gust front algorithm was 27/1146 (2.4%). None of the false alarms occurred in the airport sector, defined as the area bounded by the azimuths 240° and 10° and the ranges 0 to 30 km from the TDWR testbed radar. Therefore the pilots received no false warnings.

The POD does not indicate how well the algorithm detects a gust front. Figure 17 shows an example of a valid detection that may not be considered a good detection. A portion of the detection labeled EV9 is located within the truth box that represents a gust front identified as GF2. A valid detection is declared, but the algorithm detection overlaps less than 10% of the total length of the gust front. If *percent of length detected* is signified by POL, a minimum POL threshold (POL_{min}) can be applied so that POL must exceed the threshold before a valid detection is declared. Figure 18 shows POD plotted as a function of POL_{min}. Table 4 gives the average POL as a function of gust front strength.

The location and intensity of the wind shear constitute the wind shear warning. Location is scored by computing the number of wind shear alerts issued at the airport divided by the number of wind shear alerts that should have been issued. Table 5 shows the results of this analysis, which is termed the *probability of correctly locating gust front wind shear.*

The number of false alarms issued divided by the total number of alarms issued (3/206 or 1.5%) defines the *probability of false warning* (PFW). In these three false alarms, gust fronts were in the airport vicinity, but the detections did not agree well with the truth, and unnecessary warnings were generated. No detection in the airport sector appeared where no gust front existed.

The measures of algorithm performance shown in Tables 3 through 5 indicate that the ability of the algorithm to detect gust fronts increases with gust front strength. Thus, the algorithm is better at detecting the more hazardous gust fronts.

Wind shear intensity is scored by comparing

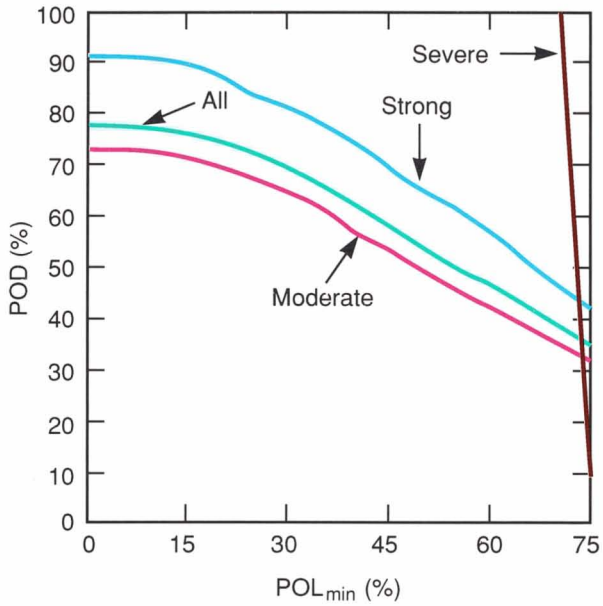

Fig. 18—Probability of detection (POD) as a function of percent-of-length-detected threshold (POL_{min}) for moderate, strong, severe, and all gust fronts.

Table 4. Average Percent of Length Detected for Gust Fronts

Moderate	*Strong*	*Severe*	*All*
66%	68%	73%	67%

the intensity expressed in the wind shear alert message to pilot reports as logged by observers in the tower. The average absolute difference between pilot reports and alerts is about 10 knots, with alerts overestimating wind shear relative to pilot reports.

An aircraft that encounters a gust front is expected to experience a gain in wind speed (Fig. 3). In some instances, however, pilots report a wind-speed loss. This fact results in a large wind-speed difference in the wind-speed error analysis. If the pilot reports of losses are removed from the analysis, the average absolute difference between pilot reports and alerts is about 5 knots. Cases in which pilots report a wind-speed loss must be studied further to determine why an inconsistency exists between the reported and estimated shears.

Effective runway management is achieved by alerting an ATC supervisor, within 20 min of arrival, when a wind shift is expected at the airport (forecasted location), and to what velocity the winds will change with its passage (wind-shift estimate). A valid forecast is declared if it falls within the truth region for the time at which the forecast is valid. If the forecast falls outside the truth box, the forecast is considered a miss. A false forecast is declared if the gust front dissipates before the validation time. The number of valid forecasts divided by the number of events for which forecasts were made gives the *probability of correct forecast* (PCF). The number of false forecasts divided by the number of events for which forecasts were made plus false forecasts gives the *probability of false forecast* (PFF). The algorithm generates a forecast for 10 and 20 min into the future. Table 6 shows the PCF as a function of gust front strength. The PFF is 11% for the 10-min forecasts and 18% for the 20-min forecasts. However, the algorithm was able to produce forecasts for only 45% of the 270 gust fronts and convergence boundaries that occurred during the 1988 test. When forecasts are generated, they are accurate; unfortunately, forecasts are not generated often.

The accuracy of the wind-shift estimate is determined by comparing the wind-shift estimate to the mesonet data. The average absolute difference in wind speed and direction between the wind-shift estimate and the mesonet data is 3 m/s and 30°, respectively. The wind-shift speed is 1.5 m/s larger, on the average, than that determined from the mesonet data (which may be explained by the difference in height of the measurements [21]). The average wind-shift direction is about 5° counterclockwise of the mesonet wind direction.

Table 5. Probability of Correctly Locating Gust Front Wind Shear

Moderate	*Strong*	*All*
64%	86%	70%

Summary

The Lincoln Laboratory program on wind shear detection has resulted in the development of a significant capability for warning pilots of imminent hazards along their approach and departure flight paths. This effort has coordinated research and development programs with other government-sponsored organizations

Table 6. Probability of Correctly Forecasting Wind Shift

	Moderate	*Strong*	*Severe*	*All*
10	94%	96%	100%	95%
20	82%	84%	0%	83%

(most notably NSSL and NCAR), resulting in an integrated system for the identification and display of hazardous wind shear and operationally significant wind shifts. Lincoln staff participated in the development of the TDWR system specification, and assisted the FAA in evaluating contract proposals for the system procurement. Several field measurement programs, particularly the TDWR OT&E at Denver in 1988, carefully assessed the performance of this system.

The results of the OT&E test and evaluation program indicate that the current wind shear and wind-shift algorithms perform well and provide a significant benefit to the safety and efficiency of terminal operations. Ongoing development and testing efforts aim to enhance the aspects of the system operation in which algorithm performance could be substantially improved.

Acknowledgments

The work described in this article is the result of several years of development and field testing performed by dozens of individuals from Lincoln Laboratory, the National Severe Storms Laboratory, and the National Center for Atmospheric Research. The authors would like to acknowledge the contributions of their Lincoln Laboratory colleagues Stephen Olson, Hayden Schultz, and Valerie Coel to the development of the real-time microburst algorithm, and Mark Isaminger, Darelyn Neilley, Richard DeLaura, Robert Hallowell, and Joseph Cullen for their efforts on single-Doppler truthing and scoring. William Mahoney and F. Wesley Wilson (NCAR) provided considerable insight and assistance on algorithm development and evaluation. Michael Eilts and Laurie Hermes (NSSL) were responsible for the development and evolution of the gust front and wind-shift algorithms, and much of the ground-truth analyses for these algorithms. This work was sponsored by the Federal Aviation Administration.

References

1. National Research Council, *Low-Altitude Wind Shear and Its Hazard to Aviation* (National Academy Press, Washington, DC, 1983).
2. M.M. Wolfson, "Characteristics of Microbursts in the Continental United States," *Lincoln Laboratory Journal* **1,** 49 (1988).
3. J.E. Evans, and D. Johnson, "The FAA Transportable Doppler Weather Radar," *Preprints, 22nd Conf. on Radar Meteorology, Zurich, 10–13 Sept. 1984* (Amer. Meteor. Soc.), p. 246 (1984).
4. J. McCarthy, J.W. Wilson, and T.T. Fujita, "The Joint Airport Weather Studies Project," *Bull. Amer. Meteor. Soc.* **63,** 15 (1982)
5. J. Dodge, J. Arnold, J. Wilson, J. Evans, and T.T. Fujita, "The Cooperative Huntsville Meteorological Experiment (COHMEX)," *Bull. Amer. Meteor. Soc.* **67,** 417 (1986).
6. J. Wilson, J. Moore, G. Brant Foote, B. Martner, A. Rodi, T. Uttal, and J. Wilczak, "Convective Initiation and Downburst Experiment (CINDE)," *Bull. Amer. Meteor. Soc.* **69,** 1328 (1988).
7. C. Biter, *TDWR/LLWSAS User Working Group, Summary of the 15–17 February 1989 Meeting,* National Center for Atmospheric Research, Boulder, CO (1989).
8. S.D. Campbell and M.W. Merritt, "TDWR Scan Strategy Requirements," *Project Report ATC-144,* Lincoln Laboratory (1988).
9. R.D. Roberts and J. Wilson, "Precipitation and Kinematic Structure of Microburst Producing Storms," *Preprints, 22nd Conf. on Radar Meteorology, Zurich, 10–13 Sept. 1984* (Amer. Meteor. Soc.), p. 71.
10. S.D. Campbell, "Microburst Precursor Recognition Using an Expert System Approach," *Proc. 4th Intl. Conf. on Interactive Information and Processing Systems for Meteorology, Oceanography and Hydrology, Anaheim, CA, 30 Jan.–3 Feb. 1989* (Amer. Meteor. Soc.), p. 300.
11. J.E. Evans, "Ground Clutter Cancellation for the NEXRAD System," *Project Report ATC-122,* Lincoln Laboratory (1983).
12. D.R. Mann, "TDWR Clutter Residue Map Generation and Usage," *Project Report ATC-148,* Lincoln Laboratory (1988).

13. S. Crocker, "TDWR PRF Selection Criteria," *Project Report ATC-147*, Lincoln Laboratory (1988).
14. M.D. Eilts and S.D. Smith, "Efficient Dealiasing of Doppler Velocities Using Local Environmental Constraints," *Environmental Research Laboratories Report*, National Severe Storms Laboratory (1989), DOT/FAA/SA-89/1.
15. M.W. Merritt, "Automated Detection of Microburst Wind Shear for Terminal Doppler Weather Radar," *Proc. Digital Image Processing and Visual Communications Technologies in Meteorology, SPIE* **846,** 61 (1987).
16. H. Uyeda and D.S. Zrnic, "Automatic Detection of Gust Fronts," *J. Atmos. and Oceanic Tech.* **3,** 36 (1986).
17. S.D. Smith, A. Witt, M. Eilts, D. Klingle-Wilson, S. Olson, J. Sanford, "Gust Front Detection Algorithm for the Terminal Doppler Weather Radar: Part I, Current Status," *3rd Intl. Conf. on Aviation Weather Systems, Anaheim, 30 Jan.–3 Feb. 1989* (Amer. Meteor. Soc.), p. 31 (1989).
18. S.D. Smith, "Sectorized Uniform Wind Algorithms," *NEXRAD Joint Systems Program Office Report*, National Severe Storms Laboratory (1986).
19. D. Turnbull, J. McCarthy, J. Evans, and D. Zrnic, "The FAA Terminal Doppler Weather Radar (TDWR) Program," *3rd Intl. Conference on Aviation Weather Systems, Anaheim, 30 Jan.–3 Feb. 1989* (Amer. Meteor. Soc.), p. 414 (1989).
20. M.M. Wolfson, J.T. DiStefano, and B.E. Forman, "The FLOWS Automatic Weather Station Network in Operation," *Project Report ATC-134*, Lincoln Laboratory (1986).
21. M.D. Eilts, "Low Altitude Wind Shear Detection with Doppler Radar," *J. Climate and Appl. Meteor.* **26(1),** 96 (1987).

MARK W. MERRITT is a staff member in the Air Traffic Surveillance group. His research interest is in the detection of aviation weather hazards by Doppler radar. He received an S.B.E.E. degree in 1981 and an S.M.E.E. degree in 1983, both from MIT. Mark has been at Lincoln Laboratory since 1981.

STEVEN D. CAMPBELL has worked for Lincoln Laboratory since 1978 in areas related to air traffic safety. He developed ground-support hardware for the TCAS aircraft collision avoidance system project, and was project engineer for the Lincoln-developed software and hardware for the GPS satellite navigation project. Since 1984, he has been working on an artificial intelligence approach to microburst recognition for the TDWR program. His current focus of interest is in microburst prediction. He received his B.S.E.E., M.S.E.E., and Ph.D. degrees in electrical engineering from the University of Washington.

DIANA KLINGLE-WILSON is a staff member in the Air Traffic Surveillance group. She received a B.A. degree in geography from Indiana University, an M.S. degree in atmospheric science from the University of Michigan, and a Ph.D. degree in atmospheric science from Purdue University. Diane also worked for the Travelers Insurance Corporation in Hartford, Conn., in the Natural Hazards Risk Assessment Program. She joined Lincoln Laboratory in 1987.